MODEL-BASED TRAJECTORY CONTROL OF PRESSURE SWING ADSORPTION PLANTS

M. Bitzer K. Graichen M. Zeitz

Institut für Systemdynamik und Regelungstechnik,
Universität Stuttgart, Pfaffenwaldring 9, 70550 Stuttgart,
Germany

E-mail: {bitzer, graichen, zeitz}@isr.uni-stuttgart.de

Abstract: Pressure swing adsorption (PSA) plants consist of several fixed-bed adsorbers and are operated as cyclic multi-step processes. PSA processes are used for the separation and purification of gas mixtures. Based on a rigorous distributed parameter model of the considered 2-bed PSA plant, a process control scheme is derived which is composed of a nonlinear feedforward control and a linear feedback control. For the design of the feedforward control, a numerical approach for the inversion of the rigorous plant model is presented. The designed trajectory control scheme is evaluated by use of the PSA plant simulation model.

Keywords: multi-step process, periodic process operation, distributed parameter system, adsorption process, nonlinear travelling concentration waves, numerical model inversion, feedforward control, feedback control.

1. INTRODUCTION

Pressure swing adsorption (PSA) is a standard process technique for the separation of gas mixtures (Ruthven *et al.*, 1994). The plants consist in general of several fixed-bed adsorbers and are operated as cyclic multi-step processes, i.e. the connections between the different adsorbers are changed by the switching of valves at the transition from one cycle step to the next. Thereby, a periodic operation is realized for the adsorption process.

In this contribution, a 2-bed pressure swing adsorption plant for the production of oxygen from air is considered. Its flowsheet is shown in Figure 1. Each fixed-bed adsorber is described by a nonlinear model with distributed parameters (Unger, 1999). The implementation of a rigorous PSA model within e.g. the simulation environment DIVA (Köhler *et al.*, 2001) enables its dynamical analysis and the evaluation of new control schemes.

A characteristic feature of PSA plants concerns the occurrence of nonlinear travelling concentration waves which are alternating their propagation direction as a consequence of the periodic process operation. In accordance with the cyclic coupling of the fixed-bed adsorbers, the occurring waves travel back and forth within the two adsorber beds and are thereby changing their shape, see Figure 1. The cycle time as well as the duration of the cycle steps do considerably affect the product concentration, because they determine the extent of breakthrough of a concentration front at the product end of the adsorber beds. The cycle time is therefore considered to be the manipulating variable of the process.

The appropriate operation of the PSA plant requires the solution of two control tasks in order to guarantee a desired purity of the product, i.e. the average concentration in the oxygen tank, see Figure 1. These control tasks comprise the stabilization of operating points as well as the trajectory control for set-point changes. The main

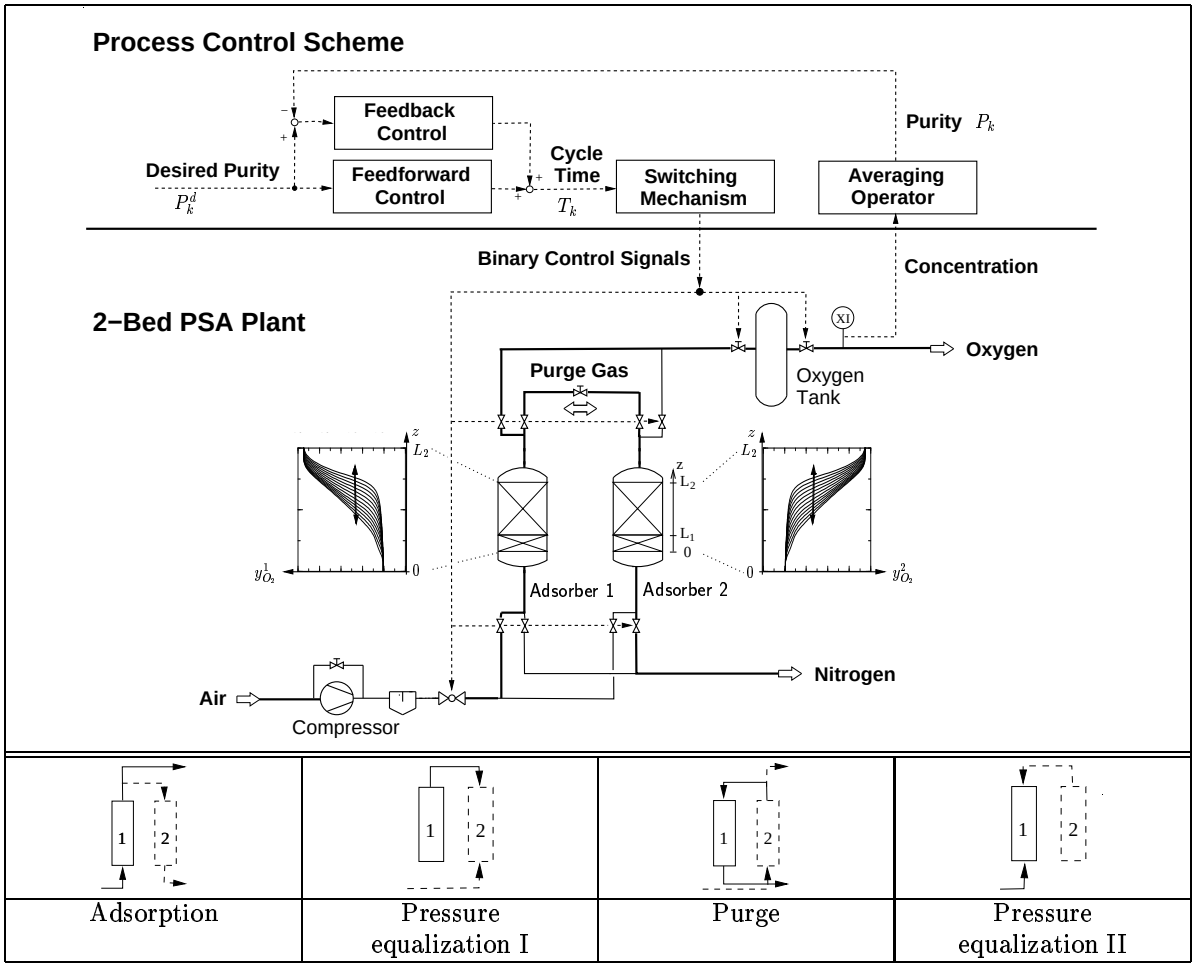

Fig. 1. Flowsheet of a 2-bed pressure swing adsorption plant for oxygen production from air with travelling oxygen concentration waves $y^i_{O_2}(z,t)$, $i \in \{1,2\}$ in both beds (middle), the coupling schemes for the adsorbers during a 4-step cycle (bottom), and the proposed process control scheme (top).

topic of this contribution is the trajectory control of the product purity. Therefore, a process control scheme is presented which consists of a feedforward control and a feedback control, see Figure 1.

The paper is organized as follows: in the next section, the model of the 2-bed pressure swing adsorption plant for the production of oxygen from air is briefly introduced and the occurring control design problem is specified. Then, an approach for the numerical model inversion used for the determination of the feedforward control is explained, the design of the feedback control is discussed, and the whole process control scheme is presented. Finally, the efficiency of the whole control concept is demonstrated by simulations with the rigorous PSA model.

2. TWO-BED PRESSURE SWING ADSORPTION PLANT

The considered 2-bed PSA plant, Figure 1, is used for the oxygen production from air for medical purposes. The produced oxygen is stored in a tank from which it is taken off by the consumer. The operation cycle consists of four steps: adsorption, pressure equalization I, purge, and pressure equalization II. The related four coupling schemes of the two adsorbers are depicted at the bottom of Figure 1.

2.1 *Nonlinear PSA plant model*

Each adsorber consists of a series connection of a prelayer and an adsorption layer with space ranges $0 \le z \le L_1$ and $L_1 \le z \le L_2$ respectively, see Figure 1. The adsorption layer model [1] considers air as a binary mixture of oxygen and nitrogen, and emanates from two phases, i.e. a gaseous and an adsorbed phase. The prelayer adsorbs moisture, which is neglected, and is therefore modeled as a gaseous phase only.

The distributed parameter model for the adsorption layer of each adsorber, $i \in \{1,2\}$ consists of six quasilinear partial differential algebraic equations for the pressure $p^i(z,t)$, oxygen mole fraction

[1] The detailed model as well as simulation results can be found in (Unger, 1999) and are also given in (Bitzer and Zeitz, 2002; Bitzer *et al.*, 2002).

Model of **adsorption layer** for each adsorber, $i \in \{1, 2\}$:

$$\text{PDAE:} \quad B\left(\boldsymbol{x}^i\right) \frac{\partial \boldsymbol{x}^i}{\partial t} = A\left(\boldsymbol{x}^i\right) \frac{\partial \boldsymbol{x}^i}{\partial z} + \boldsymbol{f}\left(\boldsymbol{x}^i\right) \quad z \in \Omega^i,\ t > 0$$

$$\text{BC:} \quad \mathbf{0} = \boldsymbol{\varphi}^j\left(\boldsymbol{x}^i, \boldsymbol{v}^i\right) \quad z \in \Gamma^i,\ t \in \vartheta_k^j$$

$$\text{IC:} \quad \boldsymbol{x}^i(z, 0) = \boldsymbol{x}_0^i(z) \quad z \in \bar{\Omega}^i$$

with state vector $\boldsymbol{x}^i = \left[p^i, y_{O_2}^i, q_{O_2}^i, q_{N_2}^i, T^i, \dot{n}^i\right]^T$,

boundary input vector $\boldsymbol{v}^i = \left[y_{O_2,in}^i, T_{in}^i, \dot{n}_{in}^i\right]^T$,

intervals $\Omega^i = (L_1,\, L_2)$, $\Gamma^i = \{L_1,\, L_2\}$, $\bar{\Omega}^i = \Omega^i \cup \Gamma^i$,

time interval $\vartheta_k^j = (t_k^j,\, t_k^{j+1}]$,

and cycle time $T_k = \sum_{j=1}^{4} \Delta t_k^j$ with $\Delta t_k^j = t_k^{j+1} - t_k^j$.

(The BCs depend on the connections between the adsorbers during the j^{th} cycle step of the k^{th} cycle, see Figures 1 and 2.)

A similar model of 4 PDAEs with BCs and ICs is given for the **prelayer**.

Model of **oxygen tank**:

$$\text{ODE:} \quad B^t\left(\boldsymbol{x}^t\right) \frac{d\boldsymbol{x}^t}{dt} = \boldsymbol{f}^t\left(\boldsymbol{x}^t, \boldsymbol{x}^i(L, t), \dot{n}_{out}^t(t)\right) \quad t > 0$$

$$\text{IC:} \quad \boldsymbol{x}^t(0) = \boldsymbol{x}_0^t$$

with state vector $\boldsymbol{x}^t = \left[p^t,\, y_{O_2}^t,\, T^t\right]^T$.

Table 1. Model of 2-bed PSA plant.

$y_{O_2}^i(z, t)$ in the gaseous phase, adsorbed amounts $q_k^i(z, t)$, $k \in \{O_2, N_2\}$, temperature $T^i(z, t)$, and molar flux $\dot{n}^i(z, t)$. The states depend on one space coordinate z and on time t.

The model of an adsorption layer can be written in vector notation (Bitzer and Zeitz, 2002) of partial differential algebraic equations (PDAEs), boundary conditions (BCs), and initial conditions (ICs) as shown in Table 1. A similar model for the prelayer is obtained by neglecting the respective terms and equations for the adsorbed amounts q_k^i, $k \in \{O_2, N_2\}$ and consists therefore of four PDAEs and respective BCs and ICs. The model of the product tank is given by three ordinary differential equations (ODEs) for the pressure $p^t(t)$, the oxygen mole fraction $y_{O_2}^t(t)$, and the temperature $T^t(t)$ (see Table 1). The output molar flow rate $\dot{n}_{out}^t(t)$ is a time-variant operational parameter which can be adjusted. For the simulation of the PSA plant model, the simulation environment DIVA (Köhler *et al.*, 2001) is used. Thereby, the model equations are spatially discretized according to the method of lines approach.

2.2 *Cyclic operation and control problem*

Each PSA plant is operated according to a specific cycle which determines the periodic operation mode of the plant. The respective operation mode represents the specific structural couplings which are associated to each step. As a consequence, the two adsorbers are operated in a phase shifted manner in order to attain a quasi-continuous production (see Figure 2). Thereby, the cycle time $T_k = \Delta t_k^1 + \Delta t_k^2 + \Delta t_k^3 + \Delta t_k^4$ is the manipulating variable of the process[2]. The controlled variable is the time-averaged purity P_k of the product, i.e. $P_{k+1} = \bar{n}_{O_2,out}/\bar{n}_{out}$ with $\bar{n}_{O_2,out} = \frac{1}{T_k}\int_{t_k}^{t_k+T_k} y_{O_2}^t \dot{n}_{out}^t\, dt$ and $\bar{n}_{out} = \frac{1}{T_k}\int_{t_k}^{t_k+T_k} \dot{n}_{out}^t\, dt$.

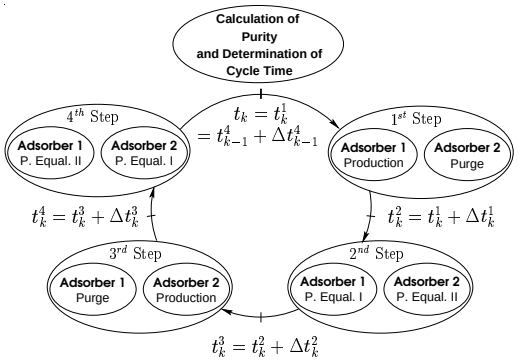

Fig. 2. Scheme of the cyclic 4-step operation of the considered 2-bed PSA plant.

PSA plants can be classified as hybrid distributed parameter systems (van der Schaft and Schumacher, 2000) with a time varying cycle time T_k, which is used as the manipulating variable. These properties have to be considered in course of the design of the process control.

3. TRAJECTORY CONTROL SCHEME

The cycle time T_k (or respectively the duration Δt_k of the cycle step times) is in general a rather unconventional manipulating variable in controller design. However, it is a natural choice for PSA plants considering their hybrid process nature. In this context, it is emphasized that 'the area of hybrid systems is still in its infancy' (van der Schaft and Schumacher, 2000). It has to be considered that such a manipulating variable is subject to constraints since a minimum amount of time is physically required for each step. An upper bound is also mandatory due to the cyclic operation of the plant itself. Bemporad and Morari (1999) suggest for instance a model predictive control framework in order to control hybrid lumped parameter systems which are modeled by linear dynamic equations and linear inequalities. Such an optimization based approach is currently too complicated for the PSA plant due to the high order of the rigorous simulation model and the related real-time problems.

[2] The cycle time T_k can be changed by Δt_k^1 and Δt_k^3, because Δt_k^2 and Δt_k^4 depend on the duration of the actual pressure equalization between the two adsorbers.

Presently, PSA plants are operated based on heuristics and the process knowledge of human operators. The proposed process control scheme comprises a feedforward control and a feedback control. The feedforward control automatizes the settings of a human operator and the feedback control is used in order to compensate disturbances and model uncertainties. The feedforward control is set up by numerically inverting the input/output (I/O) behavior of the detailed plant model [3]. The design of a feedforward control by an inverse I/O model adapts the ideas known from flatness based control applied to trajectory control of a CSTR (Rothfuß *et al.*, 1996).

In the following, the focus is first put on the cyclic and time-discrete nature of the plant, which serves for the explanation and derivation of the model inversion strategy for the design of the feedforward control. Then, the feedback control design is presented.

3.1 *Derivation of feedforward control*

Current approaches for the controller design for distributed parameter systems require the derivation of a simplified design model which captures the dominant system dynamics, see e.g. (Christofides, 2001). The cyclic operation is an intrinsic property of the process. Therefore it is certainly a shared feature of any reduced-order model which intends to approximate the PSA plant together with its cyclic and variable structure. From Figure 2, it becomes evident that the cyclic operation of the PSA plant is naturally defining Poincaré maps

$$\boldsymbol{x}_{k+1} = \boldsymbol{g}\left(\boldsymbol{x}_k, T_k\right), \quad P_{k+1} = h\left(\boldsymbol{x}_k, T_k\right) \qquad (1)$$

of the internal state $\boldsymbol{x}_k := \boldsymbol{x}(t_k)$ and the purity P_k of such a lumped reduced-order design model. This means that the state $\boldsymbol{x}_{k+1}$ and the purity P_{k+1} at the end of the k^{th} cycle depend on both the initial state $\boldsymbol{x}_k$ at the beginning of that cycle and on the cycle time T_k, which becomes an explicit variable. The iterative maps $\boldsymbol{g}(\cdot)$ and $h(\cdot)$ reflect the fundamental solution of the considered model. Their analytical calculation is therefore only possible in exceptional cases. Since the cycle time T_k is the manipulated and the purity P_k the controlled variable, these iterative maps are a time-discrete representation of the I/O behavior of the plant. PSA plants are in general operated at a periodic set-point [4] P^d, i.e. with $T_k = T^d = const.$, such that $P_k = P^d = h(\boldsymbol{x}^*, T^d)$ and $\boldsymbol{x}_k = \boldsymbol{x}^* = \boldsymbol{g}(\boldsymbol{x}^*, T^d)$. In order to perform set-point changes $P^{d,1} \rightarrow P^{d,2}$, it is necessary to follow a predetermined trajectory [5] P_k^d, $k = 0, 1, \ldots, N$ with $P_0^d = P^{d,1}$ and $P_N^d = P^{d,2}$. The I/O relation (1) is needed in order to determine the feedforward cycle time T_k^d in dependence of such a desired trajectory P_k^d. Generally speaking, the global I/O behavior of (1) needs to be inverted, i.e. $T_k^d = h^{-1}(\boldsymbol{x}_k, P_{k+1}^d)$. Such an inverse I/O relation cannot be calculated analytically, but it is identical to the solution of

$$0 = P_{k+1}^d - h(\boldsymbol{x}_k, T_k^d)\,. \qquad (2)$$

This represents an end-value problem: the cycle time T_k^d is adjusted at the beginning of each cycle while the associated purity $P_{k+1} = h(\boldsymbol{x}_k, T_k^d)$ is obtained only at the end of that cycle. This end-value problem can be calculated numerically by applying the shooting method and by using the simulation model in Table 1. The entire feedforward control sequence T_k^d, $k = 0, 1, \ldots, N$ is then calculated in a repetitive way starting from the periodic set-point $P^{d,1}$ with $\boldsymbol{x}_0 = \boldsymbol{x}^{*,1}$.

However, depending on the desired trajectory P_k^d, $k = 0, 1, \ldots, N$ and the controllability of the PSA plant, a solution T_k^d of (2) is not guaranteed. It is therefore required that the PSA plant dynamics is taken into account and that the desired trajectory is sufficiently smooth such that the plant is able to follow it. Even for very smooth desired trajectories, there may still be an individual cycle and respective desired purity increment $\Delta P_{k+1}^d = P_{k+1}^d - P_k^d$, for which no solution T_k^d for (2) exists. I.e., if there's only a single cycle during the set-point change for which no solution exists, the algorithm is not robust and a replanning of the trajectory is necessary. Therefore, in order to relax this problem, the described algorithm is reformulated. Thereby, the future dynamics is also taken into account: a moving shooting horizon [6] of $N_H > 1$ cycles is chosen. Figure 3 illustrates this situation for a horizon of $N_H = 3$ cycles. This leads to the following zero-value problem

$$0 = P_{k+N_H}^d - \bar{h}(\boldsymbol{x}_k, T_k^d, T_{k+1}^d, \ldots, T_{k+N_H-1}^d) \qquad (3)$$

of N_H variables instead of (2). The function $\bar{h}(\cdot)$ is calculated by applying (1) repeatedly. In order

[3] In a previous work, cf. (Bitzer *et al.*, 2002), a simplified model which coarsly approximates the I/O behavior of the PSA plant was used for the design of a feedforward control. The proposed strategy for the numerical inversion of the rigorous plant model allows a more precise calculation of the feedforward cycle time, especially since it is also possible to consider further important effects which were not included in the simple model previously used (e.g. a time varying output molar flow rate $\dot{n}_{out}^t$).

[4] A periodic set-point is also denoted as a so-called cyclic steady state (CSS), which means that the conditions at the end of each cycle are identical to those at its start. A numerical approach for the determination and the optimization of the CSS of periodic adsorption processes was presented by Nilchan and Pantelides (1998).

[5] The plant dynamics has to be taken into account for the planning of such a desired trajectory P_k^d, i.e. the trajectory has to be planned such that the plant is able to follow it.

[6] Similarly to model predictive control where a moving prediction horizon is used.

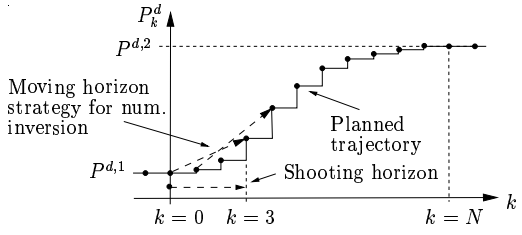

Fig. 3. Moving shooting horizon for the determination of the feedforward cycle time T_k^d and the increment ΔT_k^d.

to simplify (3), the feedforward cycle times T_k^d are chosen as $T_{k+j}^d = T_{k-1}^d + \frac{j+1}{N_H}\Delta T_k^d$, $j = 0, 1, \ldots, N_H - 1$ leading to the zero-value problem

$$0 = P_{k+N_H}^d - \tilde{h}(\boldsymbol{x}_k, \Delta T_k^d) \qquad (4)$$

for the single variable ΔT_k^d. Equation (4) is repetitively solved for ΔT_k^d as described above. The feedforward cycle time for the k^{th} cycle is chosen as $T_k^d = T_{k-1}^d + \frac{1}{N_H}\Delta T_k^d$ and the T_{k+j}^d, $j \geq 1$ are rejected. When both the desired trajectory and the shooting horizon N_H are reasonably chosen, then $h(\boldsymbol{x}_k, T_k^d) \approx P_{k+1}^d$, even though (4) is solved instead of (2). The proposed strategy therefore allows the robust numerical inversion of the detailed plant model (cf. Table 1) and the calculation[7] of a feedforward control sequence T_k^d for a transient set-point change.

3.2 *Feedback control*

In open-loop, the purity P_k is influenced due to model errors and disturbances. Therefore, a feedback control is necessary for the stabilization and robust performance of desired trajectories during set-point changes. Transferring this process control scheme to the PSA plant leads to the control block diagram shown in Figure 4.

The feedforward injection of the calculated nominal feedforward cycle time T_k^d is similar to the concept of exact feedforward linearization of flat systems (Hagenmeyer, 2003). Within the vicinity of a desired trajectory $(\boldsymbol{x}_k^d, T_k^d, P_k^d)$, the tracking error e_k of the plant can be stabilized against disturbances by a linear control law[8] $\boldsymbol{r}_{k+1} = A_c\,\boldsymbol{r}_k + \boldsymbol{b}_c\,e_k$ with the tracking error $e_k = P_k^d - P_k$ as input and the output $\Delta T_k^c = \boldsymbol{c}_c^T\,\boldsymbol{r}_k + d_c\,e_k$. The straightforward design of a PID controller by use of a simplified I/O model is discussed in (Bitzer *et al.*, 2002).

[7] Currently, the feedforward control sequence needs to be calculated offline due to the large order of the simulation model. Using the simplified model given in (Bitzer *et al.*, 2002), very good starting values for the shooting method are available and only a low number of iterations steps are necessary for each cycle.

[8] Hagenmeyer (2003) proved that the tracking error of flat and feedforward linearized systems can be stabilized by a PID like control. A prerequisite is a sufficiently smooth desired trajectory. For the PSA plant, an analytical proof is not possible due to the complex model. But, an abundant number of simulation studies showed that the I/O dynamics of the considered PSA plant is rather moderate and also stable such that it can even be locally approximated by a linear discrete model. Simulated step responses are e.g. given in (Bitzer *et al.*, 2002). Based on these considerations, the assumption that the plant can be locally stabilized by a linear controller is reasonable.

4. SIMULATION RESULTS

The validation of the proposed control concept is done by simulation studies using the rigorous simulation model. In Figure 5, the open-loop control of a set-point change scenario for the purity and a simultaneous variation of the output molar flow rate $\dot{n}_{out}^t$ is shown. It can be seen that the purity P_k pursues the desired trajectory P_k^d with an almost negligible tracking error e_k. The feedforward cycle time T_k^d is calculated by numerically inverting the detailed plant model according to (4).

The influence of a step-disturbance occurring in the output molar flow rate is shown in Figure 6 for the same set-point change scenario as in Figure 5. The simulation shows the open- as well as the closed-loop case. In the closed-loop case, the desired trajectory P_k^d is stabilized by a PID controller which was derived in (Bitzer *et al.*, 2002).

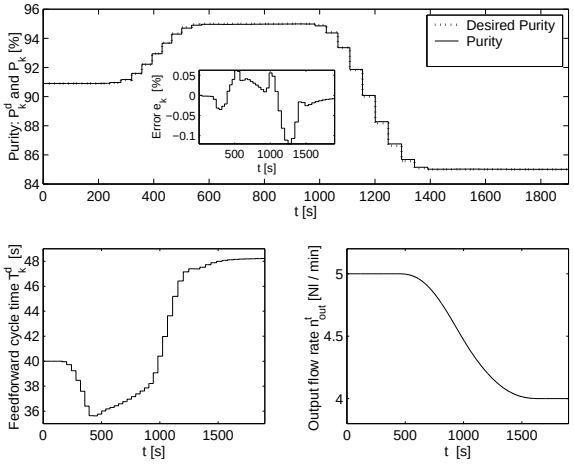

Fig. 5. Simulation of the open-loop trajectory control with a respective feedforward control sequence T_k^d calculated with a shooting horizon of $N_H = 2$. A time-variant output molar flow rate $\dot{n}_{out}^t$ is also considered.

5. CONCLUSIONS

A trajectory control scheme developed for a 2-bed PSA plant has been presented. For the feed-

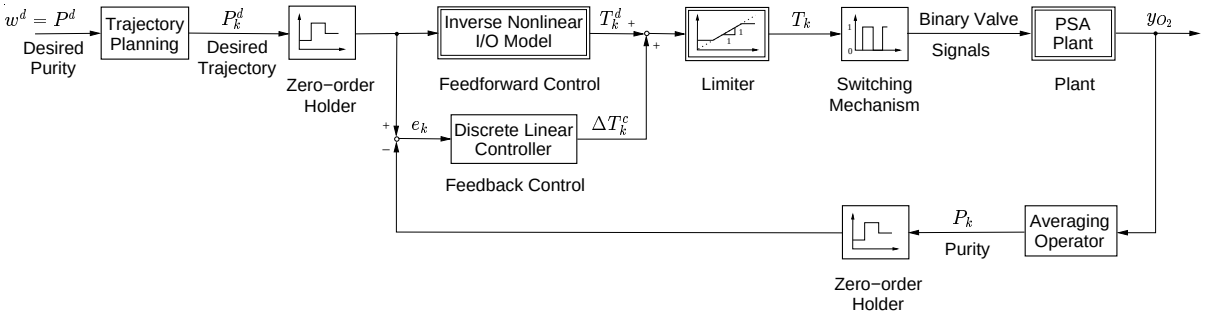

Fig. 4. Block diagram of the feedforward and feedback control for the purity P_k of the PSA plant.

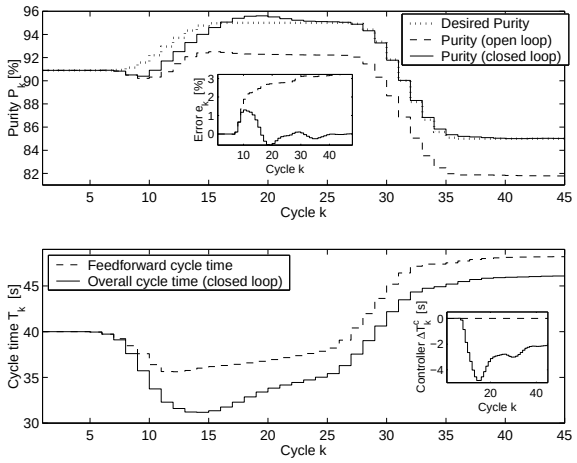

Fig. 6. Simulation of the set-point change scenario previously shown in Figure 5 subject to a step-disturbance $\Delta\dot{n}_{out}^t = +0.5\,\mathrm{Nl/min}$ superimposed to the nominal output molar flow rate and occurring at the end of the 5^{th} cycle. The open- and closed-loop case are both shown.

forward control design, a strategy for the numerical model inversion and the calculation of the inverse transient I/O behavior of the plant has been proposed. Simulation studies showed that the desired trajectory is well stabilized by a linear PID controller which is designed in a first step.

Future research will be focused on the derivation of more sophisticated reduced-order models which consider the structural changes of the process and which provide a precise representation of the internal plant dynamics. These reduced-order models will then allow real-time calculations and depending on the reduced model also the application of advanced analytical methods for the process control design.

Further issues for future research are the experimental validation (Bitzer *et al.*, 2002) of the process control concept as well as its extension to other cyclic multi-step processes, e.g. a 3-bed PSA plant (Unger, 1999).

ACKNOWLEDGEMENTS

The authors gratefully acknowledge the cooperation with Prof. G. Eigenberger, W. Lengerer, and M. Stegmaier of the *Institut für Chemische Verfahrenstechnik*. This research project is supported within *Sonderforschungsbereich 412* by *Deutsche Forschungsgesellschaft (DFG)*.

6. REFERENCES

Bemporad, A. and M. Morari (1999). Control of systems integrating logic, dynamics, and constraints. *Automatica* **35**, 407–427.

Bitzer, M. and M. Zeitz (2002). Design of a nonlinear distributed parameter observer for a pressure swing adsorption plant. *Journal of Process Control* **12**(4), 533–543.

Bitzer, M., W. Lengerer, M. Stegmaier, G. Eigenberger and M. Zeitz (2002). Process control of a 2-bed pressure swing adsorption plant and laboratory experiment. In: *CHISA 2002, 15th International Congress of Chemical and Process Engineering (CD-ROM)*. Prague/Czech Republic, August 25-29, 2002. Paper No. 833 (Also available at: http://www.isr.uni-stuttgart.de/~bitzer/).

Christofides, P. D. (2001). Control of nonlinear distributed process systems: recent developments and challenges. *AIChE* **47**(3), 514–518.

Hagenmeyer, V. (2003). *Robust Nonlinear Tracking Control Based on Differential Flatness*. Fortschritt–Berichte Nr. 8/978. VDI-Verlag, Düsseldorf.

Köhler, R., K. D. Mohl, H. Schramm, M. Zeitz, A. Kienle, M. Mangold, E. Stein and E. D. Gilles (2001). Method of lines within the simulation environment DIVA for chemical processes. In: *Adaptive Method of Lines* (A. Vande Wouwer, P. Saucez and W. Schiesser, Eds.). pp. 367–402. CRC Press. Boca Raton/USA.

Nilchan, S. and C. C. Pantelides (1998). On the optimisation of periodic adsorption processes. *Adsorption* **4**, 113–147.

Rothfuß, R., J. Rudolph and M. Zeitz (1996). Flatness based control of a nonlinear chemical reactor model. *Automatica* **32**, 1433–1439.

Ruthven, D. M., S. Farooq and K. S. Knaebel (1994). *Pressure Swing Adsorption*. VCH Publishers. New York, Weinheim, Cambridge.

Unger, J. (1999). *Druckwechseladsorption zur Gastrennung - Modellierung, Simulation und Prozeßdynamik*. Fortschritt–Berichte Nr. 3/602. VDI-Verlag, Düsseldorf.

van der Schaft, A. and H. Schumacher (2000). *An Introduction to Hybrid Dynamical Systems*. Lecture Notes in control and information sciences; 251. Springer. London, Berlin, Heidelberg, New York.

CONTROL OF GASHOLDER LEVEL BY TREND PREDICTION BASED ON TIME-SERIES ANALYSIS AND PROCESS HEURISTICS

Young-Hwan Chu[1], Jeong Hwan Kim[1], Seung Jae Moon[2], In Su Kang[2], S. Joe Qin[3], Chonghun Han[1,†]

[1]Department of Chemical Engineering, Pohang University of Science and Technology
Hyoja-Dong, Nam-Gu, Pohang, Kyungbuk, Korea 790-784
[2]Environment-Energy Team, Pohang Iron and Steel Company
Goidong-Dong, Nam-Gu, Pohang, Kyungbuk, Korea 790-300
[3]Department of Chemical Engineering, The University of Texas at Austin
Austin, Texas, USA 78712

Abstract: A novel method to control gasholder levels in an iron and steel company with accurate prediction of future trend is presented. Although various gasholders are used to recycle by-product gases generated during iron-making, coke-burning and steel-making process, the capacity of the gasholders are insufficient to handle large amount of the gases. To overcome this problem, tight control of the gasholder level should be conducted by predicting their anticipated changes. However, the current prediction logic cannot show satisfactory results due to the lack of characterization of relevant processes. In the proposed method, time-series modeling and heuristics of industrial operators are used to correctly reflect the process characteristics and deal with unexpected process delays. By applying the proposed method to an off-line data set, a significant reduction of discrepancy between predicted values and actual values has been observed. The method is expected to be adopted in the prediction system of POSCO. *Copyright © 2002 IFAC*

Keywords: Level control, Time-series modeling, Prediction, Iron and steel making process, Heuristics

1. INTRODUCTION

For iron and steel industries, it is very important to reduce energy costs due to their tremendous consumption of it. For this reason, they make every effort to recycle various materials generated from many plants (Makkonen *et al.*, 2002; Worrell *et al.*, 1997; Kim, 1998). These efforts are also significant from the viewpoint of environmental protection as well as cost saving (Sridhar *et al.*, 2002). In particular, by-product gases generated from iron-making, coke-burning and steel-making process, called as BFG (Blaster Furnace Gas), COG (Coke Oven Gas), and LDG (Linz-Donawitz Gas), respectively, are worthy of being used as a fuel since they include considerable amount of CO and H_2 (Bojic and Mourdoukoutas, 2000; Prokop and Kohut, 1998; Markland, 1980). Therefore, these gases are now being supplied to many plants via gasholders to be used as a fuel instead of expensive oil and LNG. The gasholders work as buffers that store the gases temporarily until the gas users need them as an energy source. However, due to relatively small capacity of the gasholders, overflow or lack of the by-product gases frequently occurs. As a result, many companies are interested in maintaining the levels of gasholders without severe variation for efficient utilization of the gases.

To achieve this goal, the size of the gasholders should be increased so as to mitigate the variation of the holder levels or the holder levels should be controlled in advance by predicting future levels of the gasholders based on the present patterns of gas generation and consumption. Since increasing capacity of the gasholders requires enormous costs, most steel companies are trying to solve the problem with the latter method under the management of energy center. However, most prediction logics being used in the energy center of the companies show low performance since the characteristics of the processes influencing the levels of the gasholders are not sufficiently reflected in the systems. Therefore, modification of the prediction logics is urgently required by investigating reasons for

[†] To whom correspondence should be addressed.
E-mail: chan@postech.ac.kr

the deterioration of the prediction capability and correcting the problems.

In this paper, we present new prediction logic for level changes of three gasholders in Pohang Iron and Steel Company (POSCO) based on time-series analysis and heuristics of industrial operators (Box *et al.*, 1994; Pandit and Wu, 1983). Due to practical aspects of the problem, we relied on the real data set obtained from various plants related with the by-product gases and interviews with industrial operators. This is the reason why the two techniques are mainly used in the proposed method. The time-series analysis is used to model the periodic properties of the processes connected to the BFG and COG holders. The operators' experiences are effectively utilized to know LDG generation time of next operation in the steel-making process, which is randomly changed because of frequent process delays. The randomness of the delays in the duration and occurrence time makes correct prediction of LDG holder level nearly impossible without their prior knowledge. By applying the proposed method to off-line data set, prediction performances for the three gasholders were remarkably improved. Through additional on-line test based on this success of off-line test, the proposed logic is expected to be adopted as a real system in the POSCO.

This paper is organized as the followings. In the first section, the general framework for the prediction of gasholder level in POSCO is introduced. Then, the problems of the existing logic and the features of the proposed method are given in the second section. Finally, the results of off-line application are shown in the third section followed by conclusions.

2. THEORETICAL BACKGROUND

2.1 General Framework for Prediction of Gasholder Levels.

The logics for predicting future changes of the three gasholder levels are based on the periodicity of relevant processes, although there are some exceptions depending on the processes. Therefore, if we know the cycle time, present position in the process cycle and the rate of gas generation or consumption for each interval in the cycle, we can know the future trend of gasholder level within one prediction horizon. To obtain prediction values for the holder level, prediction values for gas generation and consumption rates of relevant processes are separately calculated in advance for a prediction horizon. Once this procedure is completed, calculation of prediction values for gasholder levels is implemented according to the following algorithm. Note that different prediction methods are used for gas generation and consumption, which will be explained.

Step 1. Calculate the first prediction value by adding the first prediction value of gas generation rate to and subtracting the first prediction value of gas consumption rate from the present gasholder level.

$$l_p^1 = l_p + g_p^1 - c_p^1 \tag{1}$$

Step 2. Iteratively calculate the next prediction values based on the previous prediction value in the same way until the end of a prediction horizon.

$$l_p^n = l_p^{n-1} + g_p^n - c_p^n \tag{2}$$

where $c_p{}^n$ is n^{th} prediction value of total consumption rate at the present, $g_p{}^n$ is a n^{th} prediction value of total generation rate at the present, $l_p{}^n$ is a n^{th} prediction value of a gasholder level at the present, and l_p is a real value of a gasholder level at the present.

One prediction horizon is specified as 60 minutes for BFG and COG holders, and 40 minutes for LDG holder since these values are the cycle times of corresponding processes. The details of the prediction logic for each of the three kinds of by-product gasholders are described in the following subsections.

Trend Prediction of BFG Holder Level. BFG is generated as a by-product gas during an iron-making process. In the process, five blast furnaces (BF) are operated to make molten pig-iron and two phases are continuously repeated for each BF operation: combustion and exchange phase. Since a BFG generation rate and duration time for each phase is maintained at fixed values as shown in Fig. 1, they are set as constant parameters. Prediction of BFG generation rate is performed based on the parameters. To start prediction, we should know where the present time is located in the process cycle. For this purpose, criterion parameters with which we can know the present phase are used. Therefore, by comparing the present BFG generation rate with the criterion value, we can know the present phase in the cycle. In addition, if the starting time of the present phase is recorded, the remaining time till the end of the present phase can be known. This means that the whole prediction values for BFG generation rate within a prediction horizon can be obtained from the present time based on the parameters. It should be noted that the prediction values for total BFG generation rate are derived by adding the values of each BFG generation rate predicted for the five BFs.

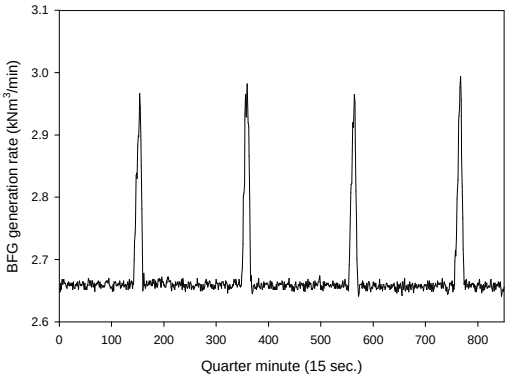

Fig. 1. Typical BFG generation pattern in BF 1.

For the case of prediction for BFG consumption rate, the following plants are considered as BFG users: five BFs, four coke ovens, twelve power plants and two hot-rolling machines. Prediction for BFG consumption rate of BFs and coke ovens is implemented in the same way as the prediction of BFG generation rate. For the other BFG-consuming plants, the present values of BFG consumption rate is merely used for prediction values within a prediction horizon since the variation of BFG consumption rate for these plants is not so severe as shown in Fig. 2 and 3.

Note that this simple approximation is possible because only small portion of the total BFG consumption rate is occupied by these plants. Once the prediction values for BFG generation and consumption rate are available, the future level changes for two BFG holders can be calculated by Eqn. (1) and (2) till the end of a prediction horizon.

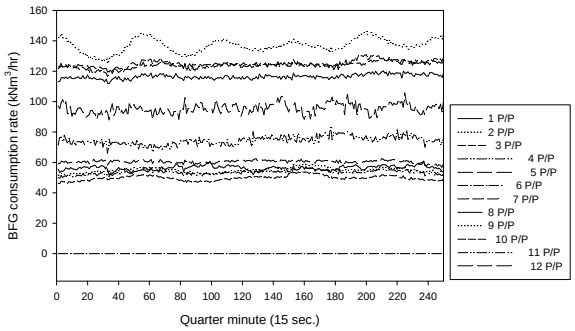

Fig. 2. Typical BFG consumption pattern for twelve power plants.

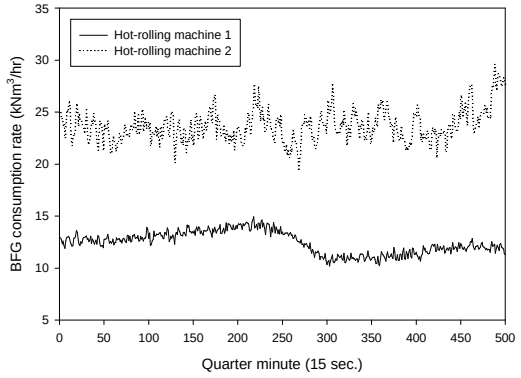

Fig. 3. Typical BFG consumption pattern for two hot-rolling machines.

Trend Prediction of COG Holder Level. COG is generated during a coke oven process. Cokes are used as a heat source for an iron-making process and they are lightly burned in the coke ovens as a preprocessing. During this process, significant amount of by-product gases are generated and they contain high percentage of CO and H_2 in themselves. Therefore, this gas is recycled as an energy source for many plants via COG holders. Unlike the BFG holders, the sizes of two COG holders are sufficiently large and much more plants are connected with the COG holders. Due to the relatively large capacity of the holders and averaging-out effect in the variation of holder level, they keep almost constant level as shown in Fig. 4. This fact means that the prediction of COG holder level is less important than those for the other kinds of gasholders since future COG holder level will be similar to the present one. For this reason, prediction logic for COG holder level is simpler than those for BFG or LDG holder level. In case of the prediction for COG generation rate, the present value is simply used for the prediction values within a prediction horizon under the condition that the present value should be in a normal range.

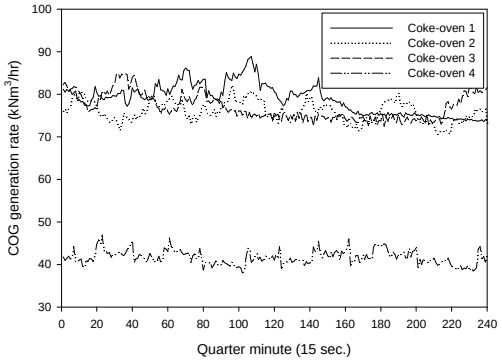

Fig. 4. Typical pattern for COG generation rate.

The plants which use the BFG as fuel also use the COG because BFG and COG is supplied to them by way of a mixing station with a specific mixing ratio. Therefore, the prediction for the COG consumption rate is implemented by multiplying the prediction values of BFG consumption rate by a ratio constant. Using the Eqn. (1) and (2), the future changes of the COG holder level can be predicted if all generation and consumption rates predicted are given to us.

Trend Prediction of LDG Holder Level. LDG is a by-product gas generated in steel-making processes. In POSCO, two steel-making plants are operated and there exists a LDG gasholder for each steel-making plant. Three converters in each steel-making plant are sequentially used to continuously produce impurity-free steel by blowing oxygen to the molten pig-iron. Although all three converters are usually operated in each steel-making plant, only two converters can be operated when one of them is under a maintenance work.

Since the steel-making process also has a periodicity, the prediction for LDG generation rate is implemented in a similar way to the cases of BFG generation rate. The only difference is that four phases exist in one cycle of the process: start of oxygen-blowing, LDG recovery, end of oxygen-blowing and tapping. LDG is generated only in LDG recovery phase and the quantity of generation is nearly constant. In current prediction logic, the time required for completion of each phase is fixed as a constant although they are frequently changed due to unexpected process delays in fact.

Therefore, significant gap between the parameters and real values for the duration time of each phase necessarily occurs and this difference causes a serious deterioration in prediction performance. We tried to solve this problem by updating the duration parameters at every process cycle based on operator's heuristics. The details will be explained in the following sections.

While the prediction for the LDG generation rate is implemented considering process characteristics, the prediction for LDG consumption rate is simple and roughly approximated as an extension of the present value since LDG consumption rate also shows no significant variation. The plants which use LDG as a fuel are the twelve power plants, two hot-rolling plants and wire-rod manufacturing plant. With the prediction values of LDG consumption and generation rate, we can obtain the prediction values for future LDG holder level, also based on Eqns. (1) and (2).

2.2 Problems of the Current Prediction Logic and the Proposed Method as a Solution.

Although we explained outline of the existing prediction logic for each by-product gasholder, there are several problems that deteriorate prediction performance. The problems are mainly caused by excessive approximation in calculating the prediction values or the fixed parameter values which should be changed according to the process condition. In fact, industrial operators have not updated the parameters for several years even if the actual process condition has changed significantly. To improve the prediction performance, we systematically analyzed the problems of the current prediction logic for each gasholder by investigating the characteristics of relevant processes based on historical data set and interviews with industry personnel. As a result, we have found out the following problems.

(a) Since the values of criterion parameters used to judge exchange phase in five BFs (both of generation and consumption) have not been updated, serious errors can be occurred in identifying the present phase. These errors make the prediction results be deviated from the actual values.

(b) In the prediction of COG generation rate, it is too simplified method to use the present value for the prediction values until the end of a horizon. Figure 4 which shows considerable variations in COG generation rate supports this fact.

(c) The pattern for BFG consumption rate in the coke oven 1 shows obvious periodicity as shown in Figure 5. Nevertheless, the current prediction logic does not consider this characteristic.

(d) The patterns for BFG and COG consumption rate in power plants and hot-rolling plants also show some variations. However, only the present value is used as prediction values for these plants in the current prediction logic.

(e) Even though actual duration time for each step in a cycle of a steel-making process severely changes depending on the process condition, they are fixed as constant parameters in calculating the prediction values for LDG generation rate. This fact leads to the prediction results very different from the real values.

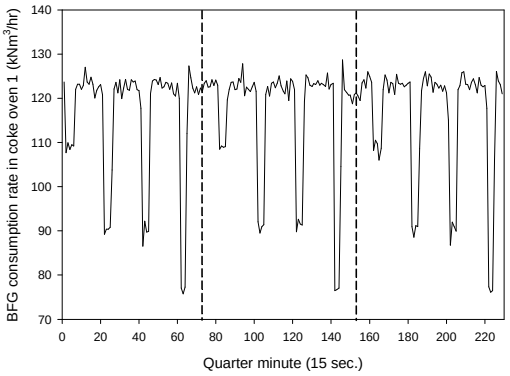

Fig. 5. Typical pattern for BFG consumption rate in coke oven 1.

We have approached these problems with time-series modeling and operator's heuristics. The schematic diagram for the proposed method together with the corresponding problems is given in Fig. 6. First of all, for the problems (b), (c) and (d), we modified the current prediction logic so that the past values can be reflected into the future values via time-series model. If the past data set is used for the prediction of future values, more robust prediction can be accomplished. Namely, although the present value includes severe noise or disturbances, the prediction values can maintain the trend continued from the past. In addition, the time-series model makes undetected past trend automatically reflected in the prediction values.

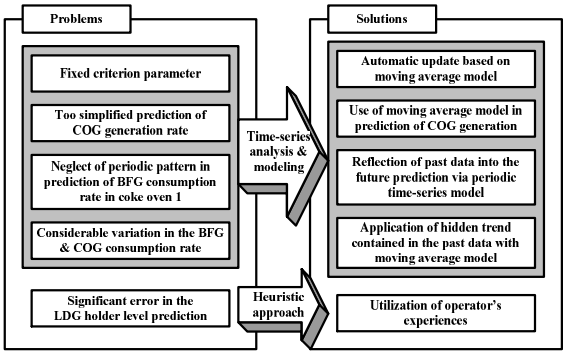

Fig. 6. Schematic diagram for the proposed method.

Of various kinds of time-series model, we used the moving average model such as Eqn. (3) for the problem (b) and (d). Although the variations for them are not so severe, we can improve the prediction performance by reflecting long-term trend of the past data into the

future prediction values with the moving average model. Note that different values are used for k (the number of the past data) depending on the characteristics of process.

$$\tilde{x}_t = x^1_{t-1} = \frac{1}{(k)} \sum_{i=t-k}^{t-1} x_i \qquad (3)$$

Meanwhile, we applied a periodic time-series model in the form of Eqn. (4) to solve the problem (c) since the same pattern is obviously repeated with specific period. Through more rigorous analysis on the actual data, the average value of the period was revealed as 20.5 minutes. Since the prediction values are obtained with 30 seconds interval, we built the periodic time-series model based on the unit of 30 seconds.

$$\tilde{x}_t = x^1_{t-1} = \frac{1}{14}(x_{t-82} + 6x_{t-81} + x_{t-42} + 6x_{t-41}) \qquad (4)$$

In this equation, the weights have been empirically determined and two previous periods have been considered to obtain more generalized results.

Problem (a) can be solved also with the moving average model such as Eqn. (3). By using the data during the past 60 minutes for this moving average model (k = 120), recent process condition can be reflected into the criterion parameters. This means that the parameters are automatically updated at each prediction.

Finally, we handled the problem (e) assisted by the heuristics of industrial operators in the steel-making process. Because of process delays occurred unexpectedly and frequently during the process, the prediction data obtained by fixed parameters give us no information on the future process trend. Therefore, we focused on how to detect the delay in advance as a crucial point of this problem. There were so many causes for the changes of the process condition and too much time and efforts were expected to perfectly consider all the process changes and build a model including all the information. Fortunately, we found out correct prediction of LDG generation rate is possible with the aid of industrial operators. It was revealed that only the operators of converters know beforehand whether the unexpected process delay occurs as well as the duration time of the delay based on their heuristic judgement resulted from the present condition of steel-making process. Therefore, we modified the current prediction logic for LDG generation rate so that the operators send the information on the process delay to energy center at each process cycle to improve prediction performance.

3. RESULTS OF OFF-LINE TEST

We applied the proposed logic to the off-line data to validate its performance. Fig. 7 shows a result of prediction at 15:00:00 on Mar. 3, 2002 based on both of the existing and the proposed logics for LDG 1 holder level. From this figure, we can see the gap between the real data and the prediction data has been remarkably reduced by using the proposed logic. In Table 1 and 2, it is shown that the proposed logic surely produces better prediction values for most cases although the degree of improvement decreases as the prediction data are far from the present.

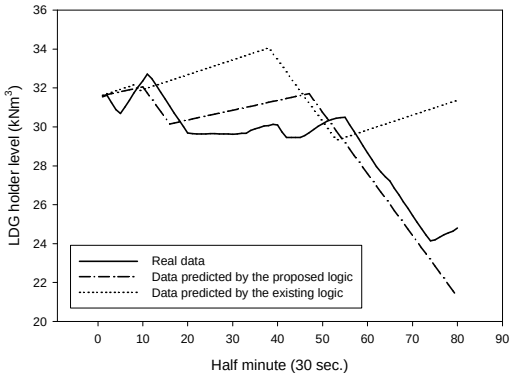

Fig. 7. Comparison between real data and both prediction data based on the existing and proposed logic for LDG 1 holder level. (implemented at 15:00:00 on Mar. 3, 2002)

4. CONCLUSIONS

In this paper, we proposed an improved logic for prediction of three kinds of by-product gasholder levels using time-series modeling and industrial heuristics. The results of off-line test showed that the proposed logic outperforms the existing logic on the average. By virtue of the success in the off-line test, the proposed logic is expected to be utilized in the actual prediction system of POSCO after rigorous on-line tests. If correct prediction of the future trend for each gasholder level is possible with the proposed logic, stable and safe management of the gasholders without waste or shortage of the gases can be achieved. Ultimately, significant reduction of energy costs via efficient use of by-product gases will contribute to enhancement of the overall productivity of POSCO.

REFERENCES

Bojic, M. and P. Mourdoukoutas (2000). Energy saving does not yield CO_2 emissions reductions: the case of waste fuel use in a steel mill. *Applied Thermal Engineering*, **20**, 963-975

Box, G. E. P., G. M. Jenkins and G. C. Reinsel (1994). *Time series analysis: forecasting and control.* Prentice Hall, Englewood Cliffs, NJ, USA.

Kim, K. (1998). Recycling technology of waste plastics in iron and steel industry. *Fuel energy abstr.*, **39**, 234

Li, C., H. Mi, W. Lee, W. You and Y. Wang (1999). PAH emission from the industrial boilers. *J. hazard. mater.*, **69,** 1-11

Makkonen, H. T., J. Heino, L. Laitila, A. Hiltunen, E. Pöyliö and J. Härkki (2002). Optimisation of steel plant recycling in Finland: dusts, scales and sludge. *Resour. conserv. recycl.*, **35**, 77-84

Markland, R. E. (1980). Improving fuel utilization in steel mill operations using linear programming. *J. oper. manage.*, **1**, 95-102

Pandit, S. M. and S. Wu (1983). *Time series and system analysis, with applications.* Wiley, New York, USA.

Prokop, L. and K. Kohut (1998). Process and apparatus for production of mixed combustion gas. *Fuel energy abstr.*, **39**, 188

Sridhar, S., D. Sichen, U. B. Pal and S. Seetharaman (2002). Abating Environmentally Harmful Waste Gases, *JOM*, **54**, 30-33

Worrell, E., L. Price, N. Martin, J. Farla and R. Schaeffer (1997). Energy intensity in the iron and steel industry: a comparison of physical and economic indicators. *Energy Policy*, **25**, 727-744

Table 1. Result of off-line test for BFG and COG holder level prediction after 1000 executions

		After 2 min.	After 4 min.	After 6 min.	After 8 min.	After 10 min.
BFG	Average difference for the existing logic (kNm^3)	4.20	6.05	6.96	8.9	10.7
	Average difference for the proposed logic (kNm^3)	2.43	2.89	3.12	3.56	3.82
	Relative improvement (%)	42.2	52.2	55.2	60	64.3
COG	Average difference for the existing logic (kNm^3)	1.07	1.9	3.0	3.6	5
	Average difference for the proposed logic (kNm^3)	0.6	1.0	1.9	2.6	3.1
	Relative improvement (%)	41.8	47.0	36.2	37.7	39.4

Table 2. Result of off-line test for LDG holder level prediction after 1000 executions

		After 10 min.	After 20 min.	After 30 min.	After 40 min.
LDG (operation only with 2 converters)	Average difference for the existing logic (kNm^3)	157.0	469.5	349.2	428.7
	Average difference for the proposed logic (kNm^3)	67.2	102.8	170.0	463.9
	Relative improvement (%)	57.2	78.1	51.3	8.2
LDG (operation with all converters)	Average difference for the existing logic (kNm^3)	534.5	2518.7	2741.0	3042.7
	Average difference for the proposed logic (kNm^3)	133.7	175.2	244.9	225.6
	Relative improvement (%)	75.0	93.0	91.1	92.6

SETTING OF INJECTION VELOCITY PROFILE VIA AN ITERATIVE LEARNING CONTROL APPROACH

Yi Yang and Furong Gao*

Department of Chemical Engineering
The Hong Kong University of Science & Technology
Clearwater Bay, Kowloon, Hong Kong

Abstract: Injection velocity is an important variable that affects the quality of injection molded products. Profiling the injection velocity to keep a constant melt-front-velocity inside the mold throughout the filling to ensure a uniform part is the purpose of this work. Based on a transducer designed in a previous work, the melt-front-position is measured online. An iterative learning control system, designed as the outer loop controller in a cascade fashion, is used to solve the optimization problem of setting the injection velocity profile. Experiments show that proposed system works well in ensuring a uniform melt-front-velocity when filling molds with varying geometrical shapes, without the necessity of a physically-based process model. *Copyright © 2002 IFAC*

Keywords: Injection molding, velocity control, cascade control, iterative learning control, product quality.

1. INTRODUCTION

Injection molding, an important cyclic polymer processing technique, transforms plastic granules into various types of products ranging from simple toys to DVD diskettes and precision lens. A injection molding process typically consists of three stages, injection of molten plastic into mold cavity (filling), packing of the material under a high pressure over a given period (packing-holding), and cooling of the polymer until it is sufficiently rigid for ejection (cooling). Filling is the first stage of the process during which the materials are forced into the mold cavity through the nozzle by the screw forward motion.

Continuous development of the molding industry finds ever-expanding applications of injection molded parts, resulting in demands for rapid production of complex parts with tight precision and superior finish. The quality of the injection molded part, typically characterized in terms of its dimensions, appearance and mechanical properties, is a strong function of the processing conditions, particularly injection velocity during the filling phase. Studies have confirmed the importance of proper setting and control of injection velocity (Johnnaber, 1985, Cox and Mentzer, 1986, Boldizar et al. 1990, and Chiu and Hsieh, 1991). Accurate control of injection velocity, to precisely follow a given velocity profile has been achieved via advanced process control strategies, for examples, by the authors (Yang and Gao, 2000 and Li et al., 2001). For a given mold and material, however, how the injection velocity should be profiled to produce the 'optimal' quality part is yet unknown. It must be clarified that the injection velocity is the velocity of the screw forward motion, which is different from the melt-front-velocity inside the mold. A schematic illustration of the mold filling is shown in Figure 1, where IV is the screw injection velocity, V_m the melt-front-velocity in the mold, A_b the cross-section area of the barrel, and A_{mf} the corresponding melt-front-area inside the mold. It is clear that the melt-front-velocity is greatly influenced by the mold geometry. Researchers in injection molding area (Hunkar, 1975, Fritch, 1979, Schmidt and Maxam, 1993, Turng et al., 1995, and Rowland and Gao, 1994) have all

* Corresponding author: E-mail: kefgao@ust.hk; Tel: +852-2358-7139; Fax: +852-2358-0054

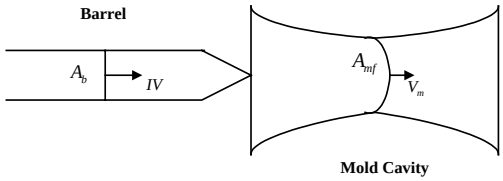

Figure 1 Schematic of mold filling

recommended that a constant melt-front-velocity during mold cavity filling should be used to profile injection velocity, to minimize non-uniformity within the molded part. This, however, cannot be implemented due to the lack of a practical melt-front flow rate measurement method.

Recently, a patented transducer has been developed to measure melt front position (MFP) during mold filling by Gao and Chen (Chen, 2002). The sensor output is linear to the melt-flow-front position within the mold. As melt-front-velocity is, simply, the derivative of the MFP, with such a transducer, the constant melt-front-velocity strategy can be translated to control the MFP to follow a constant ramp profile, as illustrated in Figure 2, where a cascade control is adopted. Consisting of two control loops, an inner injection velocity control loop that has been developed in the previous works, and an outer control loop that determines the injection velocity for the inner velocity controller. The ramp rate is the melt-front-velocity. Many existing control designs may be used for the outer loop controller, but they all require the development of a dynamic model relating injection velocity to MFP. Effort of establishing such a model based on the fundamental principles is tremendous, where the mold geometry factors and the complicated flow and material properties have to be involved. The development of such a model based on identification is inappropriate either, as this identified model will be mold dependent.

In view of the cyclic nature of the process, a model-free iterative learning control (ILC) method (detailed survey of ILC can be found in Moore and Xu (2000)) is explored here to control the MFP without having to develop a detailed process model. The ILC, which is simple in control formulation, has found many applications for cases where detailed process knowledge is unavailable. In such a control system, information of last cycle is used to improve the control of the current cycle. The controller can be removed after a number of cycles when a proper consistent profile has been obtained for the inner velocity control loop.

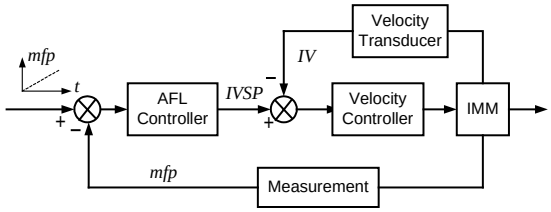

Figure 2 Block diagram of the cascade melt-flow-velocity control system

2. ILC BACKGROUND

ILC, motivated to mimic human learning process, is originally developed for the manipulation of industrial robots, in which it is required to repeat a given task with high precision. By using the repetitive nature of the processes, ILC progressively and iteratively improves the control accuracy cycle by cycle (Arimoto *et al.*, 1984). Recently, ILC has been applied to many repetitive processes, such as batch reactor, batch distillation, and injection molding (Havlicsek and Alleyne, 1999, and Gao *et al.*, 2002). In this work, the ILC approach is adopted to find a proper injection velocity profile to ensure the filling of mold cavity at a uniform melt-front-velocity.

Among many types of learning control laws proposed, a P-type learning control law is possibly the simplest, as formulated below:

$$u_{i+1}(t) = u_i(t) + L_P e_i(t) \qquad (1)$$

where $u(t)$ is the process input at time t, $e = y_s - y_m$ is the error between the output set point and real measurement; subscripts i and $i+1$ denote the cycle number and L_P is the ILC gain. It is clear that the control of the current cycle is based on the process input and the error of the last cycle in a point-to-point manner. Up to now, most of the ILC results are for the systems without time-delay. However, for many batch chemical processes such as injection molding, the effects of time delay cannot be ignored. There is a large delay between the injection velocity and the melt-front-velocity response. During injection, there exist some melt between the injection screw and the melt flow front, and the polymer melt is compressible due to its complicated visco-elastic properties. Changes in the injection velocity cannot affect the melt front flow rate instantaneously. Furthermore, the melt inside the mold cavity freezes while filling. With the development of the melt flow, the frozen layer also expands in its length and thickness, and this in turn causes increases in the delay between the injection velocity and the melt front flow rate. The long process delay as well as variations of delay during filling makes it difficult to apply the simple point-to-point ILC method. To solve this problem, control law (1) can be modified to taken into consideration of the delay term:

$$u_{i+1}(t) = u_i(t) + L_P e_i(t + t_d) \qquad (2)$$

where t_d is an estimated delay time. In this equation, the control error at time $t + t_d$ is used to update the control input at time t for the next cycle. Control law of equation 2 can be applied to cases where the time delay is exactly known. For processes with an uncertain delay, there is no guarantee that this control law will be convergent.

For a system with a varying delay bounded by h, Park *et al.* (1998) proposed to hold the control input at a constant value over the duration h, resulting a modified learning control law as below:

$$u_{k+1}(t) = u_k(mh) + \Gamma e_k(mh + dh + \xi), \quad \forall t \in [mh, mh + h), m \in \{0,1,..., M - d\} \tag{3}$$

where $e_k(mh + dh + \xi) = y_d(mh + dh + \xi) - y_k(mh + dh + \xi)$, ξ is the initial remainder, $dh + \xi$ the upper limit of delay. The system divides the process time span by the size of the time delay uncertainty h. It has been shown that the convergence can be maintained by this method (Park et al., 1998). This idea is adopted by this work. Several modifications have to be made as detailed below, considering practical issues of the process.

2.1 Division of injection velocity profile

The first modification is on the division of the filling stage time span. For a given mold, a given amount of melt needs to be injected. Changes of injection velocity profile by the ILC makes the total filling time span to vary from cycle to cycle. This creates difficulties for the division of the filling time span. Furthermore, time delay is a strong function of injection velocity, a slower injection velocity results in a larger time delay. The amount of material injected into a mold can be reasonably well represented by the distance that the screw has travelled during injection, known as injection stroke. The injection stroke is therefore used to replace the time for the ILC implementation. With this change, the time delay has also been transformed into stroke delay. As can be seen in the experimental section, the use of stroke to replace time for the ILC implementation can result in a more consistent delay for the injection stage.

2.2 Change of controlled variable

This work uses the slope of the MFP instead of MFP itself, as the controlled variable. Even though the derivative of MFP can give melt-front-velocity, it also results in a low signal-to-noise ratio. The velocity is thus obtained by linear curve fitting of MFP measurements as the following equation:

$$D_m = V_m dt + D_{m0} \tag{4}$$

where D_m is the MFP, V_m is the slope of D_m, i.e. the melt-front-velocity.

2.3 Change of manipulated variable

For most molding machines, the velocity profile can only be set in a piecewise form as illustrated in Figure

Figure 3 A typical ramp injection velocity set point profile

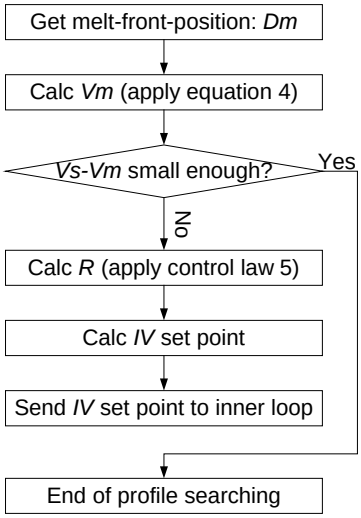

Figure 4 Flow chart of profile searching by ILC

3. It is desirable to use ramp profiles instead of step change profiles, as the step change injection velocity causes abrupt changes in MFP response, which is not desirable in this case. It is therefore decided to use the velocity ramp slope as the manipulated variable for the outer loop.

Considering all the above practical issues with injection molding, the ILC control for searching optimal injection velocity profile can be reformulated as:

$$R_{i+1}(n) = R_i(n) + L_P e_i(n + n_d) \tag{5}$$

where $R_i(n)$ is the velocity slope at n th stroke step of the i th iteration. n_d the stroke delay, $e(n + n_d) = V_s(n + n_d) - V_m(n + n_d)$, other symbols are the same as equation 3. Figure 4 shows the overall profile searching scheme via ILC approach. The slopes of injection velocity settings are obtained by control law (5), before it is reconstructed as the real injection velocity set point for the inner loop control.

3. EXPERIMENTAL SETUP

3.1 Machine and instrumentation

The molding machine used is a Chen Hsong reciprocating screw injection molding machine, model JM88MKIII. The maximum machine clamping force is 88 ton, and the maximum shot weight is 128 g. A Temposonics series III displacement/velocity transducer, type RH-N-0200M, is installed to measure the injection displacement and velocity. An in-house designed circuit is developed to convert the MFP signal into voltage signal for measurement. The hydraulic system has been fitted with a MOOG servo valves, type J661-141, to control the injection velocity. A Pentium 133MHz PC is used as the control platform for the control of the injection molding machine. Two National Instruments data acquisition cards mounted in the PC are used to provide interface to the machine. All the programs are developed using C language under a real-time multi-task operating system, the QNX. The material used in this project is high-density polyethylene (HDPE) (SABIC Ladene).

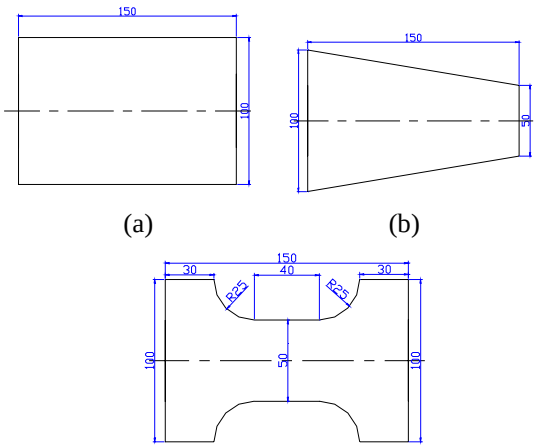

(a) (b)

(c)

Figure 5 Geometry of molds (a) mold insert 1, (b) mold insert 2 and (c) mold insert 3

3.2 Experiment Conditions

All the experiments are conducted with the barrel front heater temperature of 200°C. Three mold inserts with significant changes in geometry are used to test the control system, as illustrated in Figure 5. The sampling period for inner-loop velocity control is 5 milliseconds. The details about adaptive control of injection velocity for the inner loop can be found in references of Yang and Gao (2000) and Li *et al.* (2001).

4. RESULTS & DISCUSSIONS

4.1 Open loop test results

The first experiment is conducted with a constant injection velocity of 25mm/s. The responses of MFP measurements for three different molds of Figure 5 are shown in Figure 6. It is clear that with a constant injection velocity, melt-front-velocity varies with the changes in mold geometry. This indicates the necessity of profiling the injection velocity. The oscillations of MFP in Figure 6 are caused by capacitance measurements.

The second experiment is conducted with mold 3 to demonstrate the delay variation. As shown in Figure 7, the MFP responses are obtained, one with a constant injection velocity of 25mm/s (dotted line),

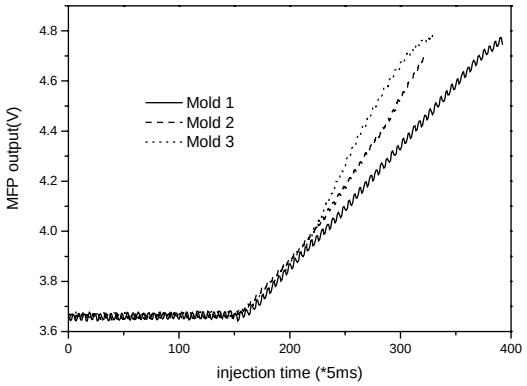

Figure 6 MFP open-loop test using different molds

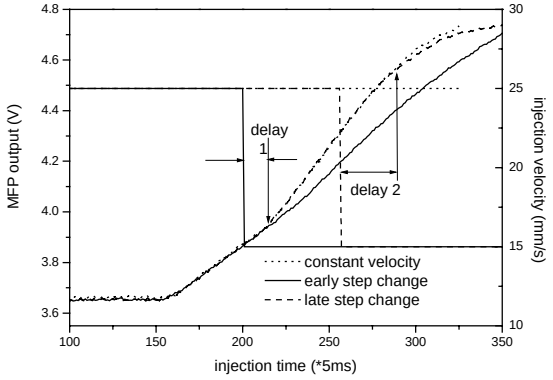

Figure 7 Illustration of the time delay variation

one with a step change injection velocity profile of 25-15mm/s with the step change introduced at 1000ms injection time (solid line), and one with the same step change profile but different step time of 1275ms (dashed line). Take the MFP response of constant injection velocity as the reference, the point where the MFP measurement begin to diverse from the reference line can be considered to be the starting time of step change response, and the time difference between step change time and the starting response time is the time delay. It can be seen from Figure 7 that the late step change obviously has much larger than delay than the early step change. The time delay changes not only with the melt flow development but also with injection velocity. The measurements are treated differently by using the injection stroke as the x-axis. The results are shown in Figures 8a (early step change) and b (late step change). The delay variation

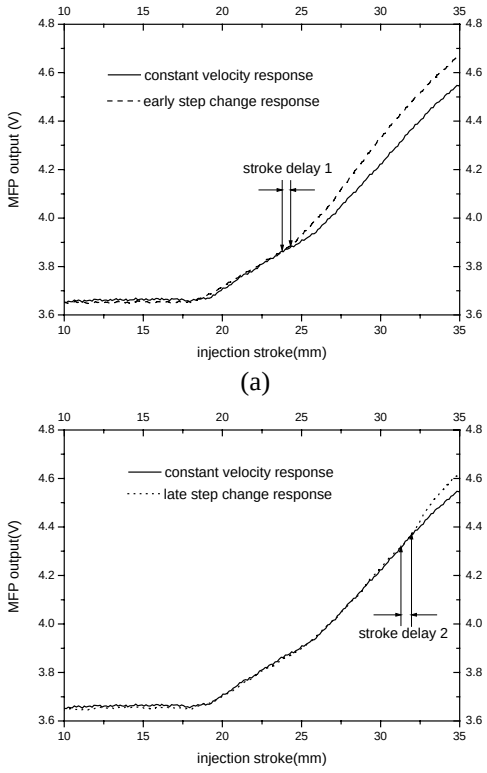

(a)

(b)

Figure 8 Illustration of delay in terms of stroke (a) delay 1: early step change and (b) delay 2: late step change

in stroke shown in Figure 8 is obviously much smaller than the delay in time of Figure 7, indicating the advantage of using the stroke.

4.2 Implementation of the ILC approach

The first step in the ILC controller design is to determine the number of steps for the filling stage. Previous works suggests that five steps of velocity profile are sufficient to achieve a satisfactory constant melt-front-velocity (Chen, 2002). Considering the fact that most injection molding machine provide 10 points injection velocity setting, i.e., 9 steps of velocity profile, so, it has been decided to use 9 steps for the velocity profiling in this work. The second issue is to determine the learning gain L_P. A large gain causes strong changes in the velocity setting and faster convergence rate, while a small gain results in a smaller change of velocity profile and a slower convergence rate. L_P has been determined to be 35 for this work after trail and error. The set point for MFP slope, V_s, is selected to be 1.0 in equation 5. The stroke delay term, n_d, is determined to be one step by the above open loop test results.

4.3 ILC search results and discussions

To illustrate the problem with the straight forward application of the point-to-point ILC of equation 2, experiment is conducted with the injection velocity settings directly adjusted by the error between the MFP set point and measurement. The resulted melt-front-position responses are shown in Figure 9a, with

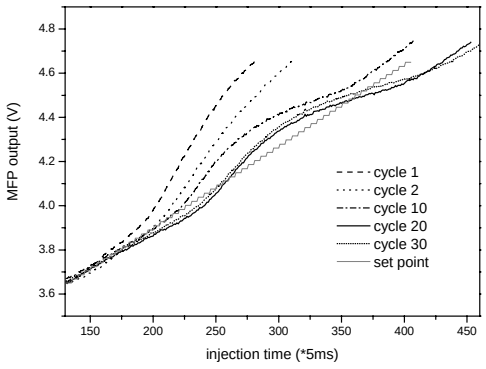

(a)

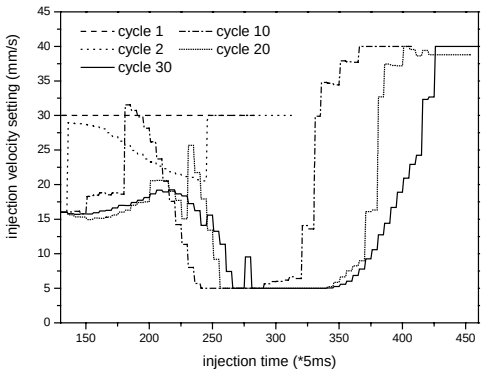

(b)

Figure 9 Point-to-point direct iterative searching of the injection velocity setting (a) MFP responses and (b) corresponding velocity settings

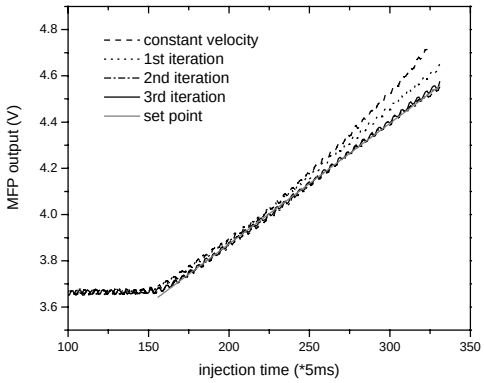

(a)

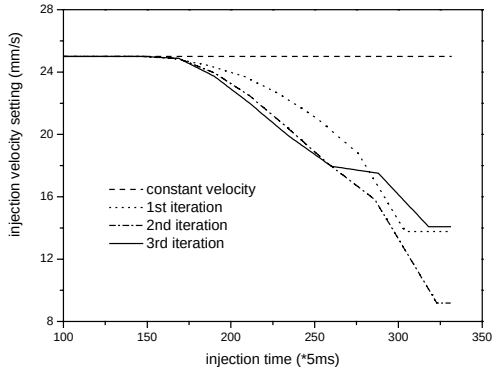

(b)

Figure 10 Experimental test of proposed ILC searching method on mold 2: (a) MFP responses and (b) corresponding velocity settings

the corresponding velocity settings shown in Figure 9b. It is clear that the MFP is far from a straight line even after 30 learning cycles, indicating that the point-to-point direct learning method cannot work well. No significant improvement can be made with changes in learning rates.

The proposed search method as ILC control law (5) is thus tested on mold insert 2. The injection stroke for filling this mold is 37.5mm. This stroke is divided into 9 steps as [16.50, 18.83, 21.17, 23.50, 25.83, 28.17, 30.50, 32.83, 35.17, 37.50], where 16.50 is the starting point when the melt front reaches the transducer. Figure 10a shows the measurement throughout 3 iterations of learning. The initial injection velocity is set to be a constant of 25mm/s. The corresponding MFP response, as indicated by the dashed line, accelerates due to the continuous decreasing of the mold cross-section area. After only two iterations, the third cycle's MFP response, shown by the black solid line, overlaps well with the set point (grey solid line). The corresponding injection velocity profiles are shown in Figure 10b. Clearly, a decreasing velocity profile, as shown in the solid line of Figure 10b, can deliver a uniform filling of mold insert 2.

The mold 3 with stronger changes in the mold shape is used to test further the designed profile searching scheme. The injection stroke is divided differently as [16.5, 19.0, 21.5, 24.0, 26.5, 29.0, 31.5, 34.0, 36.5, 39.0], due to the mold change. The ILC search

scheme is applied to this new mold without any other changes. Again, the initial injection velocity is set to be a constant 25 mm/s. The MFP responses are plotted Figure 11a. It is clearly shown that after three iterations, the MFP response is very close a straight line. The corresponding velocity profiles are shown in Figure 11b. Due to the delay, the velocity setting after 350 samples has no effect on the MPF response, and it was thus set to be constant as shown in Figure 11b.

5. CONCLUSIONS

The necessity of profiling the injection velocity to keep a constant melt-front-velocity throughout filling to produce uniform injection molded parts is demonstrated. An ILC is modified to search an "optimized" injection velocity profile to ensure the filling of mold cavity at a uniform rate, without the need of developing a process mold. The proposed system has been successfully applied to two molds with significant changes in geometry.

REFERENCES

Arimoto, S., Kawamura, S., & Miyazaki, F. (1984). Bettering operation of robots by learning. *Journal of Robotic Systems*, **1**, 123.

Boldizar A., Kubat J., and Rigdahl M. (1990). Influence of mold filling rate and gate geometry on the modulus of high pressure injection-molded polyethylene. *J. Appl. Polym. Sci.*, **39**, 63.

Chen X. (2002). A study on profile setting of injection molding. *Ph.D. Thesis.* The Hong Kong University of Science & Technology, Hong Kong, P. R. China.

Chiu C. P., and Wei J. H. (1991). Dynamic modeling of the mold filling process in an injection molding machine. *Polym. Eng. & Sci.*, **31**, 1417.

Cox H. W., and Mentzer C. C. (1986). Injection molding: the effect of fill time on properties. *Polym. Eng. Sci.*, **26**, 488.

Fritch L. W. (1979). ABS cavity flow-surface orientation and appearance phenomena related to the melt front. *SPE ANTEC Paper*, **21**, 15.

Gao F. and Chen X., USA patent application pending (2002).

Gao F., Yang Y., and Shao C. (2001). Robust Iterative Learning Control with Applications to Injection Molding Process. *Chemical Engineering Science*, **56**, 7025.

Havlicsek, H., & Alleyne, A. (1999). Nonlinear control of an electrohydraulic injection molding machine via iterative adaptive learning. *IEEE/ASME Transactions on Mechatronics*, 4, *312-323.*

Hunkar D. B. (1975). The interdependence of part parameters on process control adjustable functions in injection molding of thermoplastics. *SPE ANTEC Paper*, **21**, 161.

Johnnaber F. (1985), *Injection Molding Machines* (2nd Edn.), Hanser Publishers.

Li M. Z., Yang Y., Gao F. and Wang F. L. (2001). Fuzzy Multi-model Based Adaptive Predictive Control and its Application to Thermoplastic Injection Molding. *Canadian Journal of Chemical Engineering*, **79**, 263.

Moore K. L., and Xu J. X. (ed.) (2000). *Iterative Learning Control.* Taylor and Francis, London.

Rowland J. C., and Gao F., On-line quality monitoring coupling computer analysis and actual measurement. *Japanese Society of Polymer Processing*, Tokyo, Japan, June.

Schmidt L. R., and Maxam J. L. (1993). The influence of variable injection rate on residual stress, haze patterns and surface properties of ABS moldings. *SPE ANTEC Paper*, **39**, 1070.

Turng L. S., Chiang H. H., and Stevenson H. H. (1995). Optimization strategies for injection molding. *SPE ANTEC Paper*, **41**, 668.

Yang, Y. and Gao, F. (2000). Adaptive Control of the Filling Velocity of Thermoplastics Injection Molding. *Control Engineering Practice*, **8**, 1285.

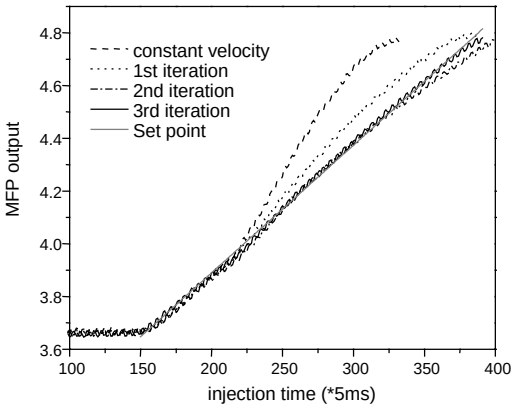

(a)

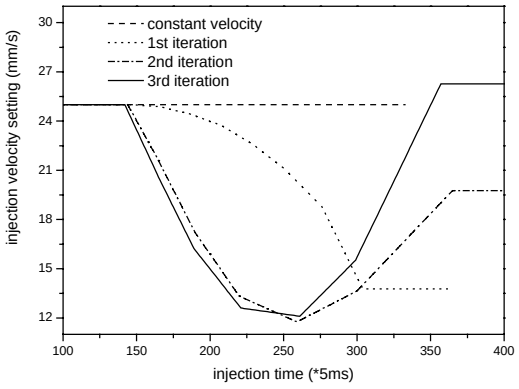

(b)

Figure 11 Experimental test of proposed ILC searching method on mold 2: (a) MFP responses and (b) corresponding velocity settings

DYNAMICS OF PROCESS NETWORKS WITH RECYCLE AND PURGE: TIME SCALE SEPARATION AND MODEL DECOMPOSITION

Michael Baldea * **Prodromos Daoutidis** * **Aditya Kumar** **

* *Department of Chemical Engineering and Materials Science, University of Minnesota, Minneapolis, MN 55455*
** *GE Corporate Research and Development, P.O. Box 8, Schenectady, NY 12301*

Abstract: Process networks with recycle are well-known to exhibit complex dynamics and to present significant control challenges, due to the feedback interactions induced by the recycle streams. In this paper, we address the dynamic analysis and control of process networks with recycle and small purge streams used for removal of light inert components (feed impurities and/or reaction byproducts) from the recycle loop. We establish, through a singular perturbation analysis, that such networks exhibit a time scale separation in their dynamics, with the slow dynamics induced by the small amount of inert purged from the recycle loop. We also present a model reduction method for deriving a nonlinear low-order model of this slow dynamics which can be used to rationally address the control of the level of inerts in the network.

Keywords: singular perturbations, DAE systems, model reduction, nonlinear control

1. INTRODUCTION

Process networks consisting of reaction and separation units interconnected through material and energy recycle are the rule rather than the exception in the process industries. The dynamics and control of such networks present distinct challenges, since in addition to the nonlinear behavior of the individual units, the feedback interactions among these units, induced by recycle, typically give rise to more complex overall network dynamics (e.g. (Morud and Skogestad, 1994; Mizsey and Kalmar, 1996; Morud and Skogestad, 1998; Jacobsen and Berezowski, 1998; Bildea and Dimian, 1998; Bildea *et al.*, 2000; Pushpavanam and Kienle, 2001; Kiss *et al.*, 2002)). Design modifications (e.g. adding surge tanks between different units to attenuate disturbances propagating through the recycle) can in principle be employed to minimize these interactions, but these are not favored by the recent demands for lower capital and operating costs, and tighter process integration. At the same time, the efficient *transient operation* of such networks is becoming increasingly important, as the current environment of frequent changes in market conditions and economical objectives dictates frequent changes in operating conditions and targets (e.g. product grade transitions, feed switching, etc.) and tighter coordination of the plant-wide optimization and advanced control levels (Marquardt, 2000; Kulhavy *et al.*, 2000). A major bottleneck towards analyzing, optimizing and better controlling the dynamics of such networks is the often overwhelming size and complexity of their dynamic models, which make dynamic simulation computationally intensive, and the design of fully centralized nonlinear controllers on the basis of entire network models impractical (such controllers are almost invariably difficult to tune, expensive to implement and maintain, and sensitive to modeling er-

[1] Partial support for this work by ACS-PRF 38114-AC9 and NSF-CTS 0234440 is gratefully acknowledged

rors and measurement noise). Indeed, the majority of studies on control of networks with recycle (see e.g. (Luyben, 1993; Luyben and Floudas, 1994; Lyman and Luyben, 1996; Yi and Luyben, 1997)) are within a multi-loop linear control framework. In a different vein, a formal framework for stability analysis and stabilization of process networks, based on passivity and concepts from thermodynamics, was recently postulated in (Farschman *et al.*, 1998; Hangos *et al.*, 1999). The development of a systematic framework for analyzing the nonlinear dynamic interactions induced by recycle structures, and rationally accounting for them in the controller design clearly remains an important open problem.

In our previous work (Kumar and Daoutidis, 2002), we considered process networks with large material recycle compared to throughput. Within the framework of singular perturbations we established that the large recycle induces a time scale separation, with the dynamics of individual processes evolving in a fast time scale with weak interactions, and the dynamics of the overall system evolving in a slow time scale where these interactions become significant; this slow dynamics is usually nonlinear and of low order. Motivated by this, we proposed: i) a model reduction methodology for deriving nonlinear low-order models of the slow dynamics induced by large recycle streams, and ii) a controller design framework comprising of properly coordinated controllers in the fast and the slow time scales.

In this paper we focus on process networks with a recycle stream *and* a purge stream. The latter is typically used for the removal of inert components (feed impurities and/or reaction byproducts); the presence of the recycle can lead to accumulation of such inert components in the recycle loop, which can in turn be detrimental to the process operation (e.g. catalyst poisoning in the reactor) and the process economics (Belanger and Luyben, 1998; Luyben, 2000). Understanding the dynamics of the inert components is therefore critical and controlling the level of such components in the recycle structure can be a key operational objective.

In almost all such networks with purge streams, the magnitude of these streams is significantly smaller than the one of the throughput and/or the recycle streams, so that raw materials losses and/or pollution can be minimized. This suggests the possibility of a "core" dynamics over a much slower time scale compared to the dynamics of the individual process units and possibly the overall network dynamics. Developing an explicit nonlinear model of this slow dynamics can be beneficial both for analysis and evaluation purposes, and for model-based control.

Motivated by the above, we consider a prototype network comprising of a reactor (with gas effluent) and a separation system, with a gas recycle stream and a purge stream to remove the light inert components. Within the framework of singular perturbations we establish that such a network does exhibit a time scale separation, with the slow dynamics associated with the small purge flowrate. Furthermore, we describe a model reduction procedure which leads to an explicit nonlinear model of this slow dynamics, suitable for analysis and control, and highlight the analogies between the case of small purge and the case of large recycle treated in our previous work.

2. MODELING OF PROCESS NETWORKS WITH RECYCLE AND SMALL PURGE

Consider the network of a gas phase reactor and a condenser shown in Fig. 1.

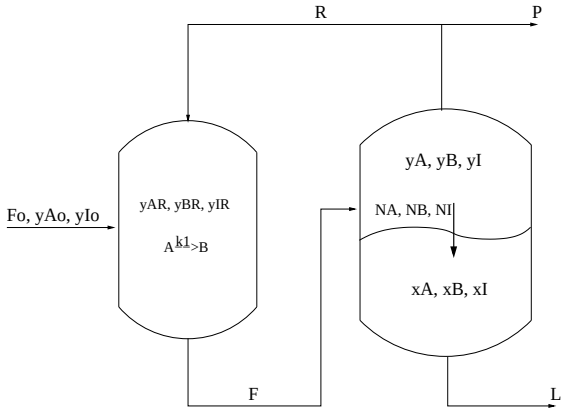

Fig. 1. Process network with recycle and purge.

Reactant A is fed at a molar flowrate F_o to the reactor, where a first-order irreversible reaction $A \rightarrow B$ takes place with a reaction rate constant k_1. The outlet stream from the reactor is fed to a partial condenser that separates the light unconverted reactant A from the heavy product B. The gas phase, rich in A is recycled back to the reactor. It is also assumed that a very volatile impurity I is present in the feed stream in small quantities. A (small) purge stream P is therefore used to remove this impurity from the recycle loop. The interphase mole transfer rates for the components A, B, I in the condenser are governed by rate expressions of the form: $N_j = k_j\alpha \left(y_j - \frac{P_j^S}{P} x_j \right)$, where $k_j\alpha$ denotes a mass transfer coefficient, y_j the mole fraction in the gas phase, x_j the mole fraction in the liquid phase, P_j the saturation vapor pressure of the component j (determined with an Antoine type relation) and P the pressure in the condenser. Assuming isothermal operation, the dynamic model of the network can be easily derived and has the form:

$$
\begin{aligned}
\dot{M}_R &= F_o + R - F \\
\dot{y}_{A,R} &= \frac{1}{M_R}[F_o(y_{0A} - y_{A,R}) + R(y_A - y_{A,R}) \\
&\quad -k_1 N_R y_{A,R}] \\
\dot{y}_{I,R} &= \frac{1}{M_R}[F_o(y_{0I} - y_{I,R}) + R(y_I - y_{I,R})] \\
\dot{M}_V &= F - R - N - P \\
\dot{y}_A &= \frac{1}{M_V}[F(y_{AR} - y_A) - N_A + y_A N] \\
\dot{y}_I &= \frac{1}{M_V}[F(y_{IR} - y_I) - N_I + y_I N] \\
\dot{M}_L &= N - L \\
\dot{x}_A &= \frac{1}{M_L}[N_A - x_A N] \\
\dot{x}_I &= \frac{1}{M_L}[N_I - x_I N]
\end{aligned} \tag{1}
$$

where $N = N_A + N_B + N_I$ and M_R, M_V, M_L denote the molar holdups in the reactor, vapor phase in the condenser and liquid phase in the condenser, respectively.

In order to facilitate a perturbation analysis of this model, the following assumptions are also introduced:

- The flowrates in the recycle loop are assumed to be $O(1)$.
- The ratio of the purge to the feed flowrate under steady state conditions is very small, or $\frac{P_s}{F_{os}} = \epsilon << 1$.
- The mole fraction of the inert in the feed is very small, or $y_{I0} = \alpha_I \epsilon$ where α_I is $O(1)$.
- The mass transfer rate for the inert component is very small, or $k_I a = \alpha_1 \epsilon^2$ where α_1 is $O(1)$.
- The inert is very volatile, or $\frac{P_I^S}{P} = \alpha_2 \frac{1}{\epsilon}$ where α_2 is $O(1)$.

Note that, based on steady state considerations, in order to remove an appreciable amount of the inert component from the recycle loop, the mole fraction of the inert in the vapor phase in the condenser, y_I, has to be $O(1)$. This implies that $O(\epsilon)$ moles of inert enter and leave the system through the feed and purge streams. Note also that the last two assumptions imply that negligible amount of inert leaves the recycle loop and exits through the liquid stream from the bottom of the condenser.

Based on the assumptions above, the dynamic model of the network takes the form:

$$
\begin{aligned}
\dot{M}_R &= F_o + R - F \\
\dot{y}_{AR} &= \frac{1}{M_R}[F_o(1 - \alpha_I \epsilon - y_{A,R}) \\
&\quad +R(y_A - y_{A,R}) - k_1 N_R y_{A,R}] \\
\dot{y}_{IR} &= \frac{1}{M_R}[F_o(\alpha_I \epsilon - y_{I,R}) + R(y_I - y_{I,R})] \\
\dot{M}_V &= F - R - (N_A + N_B) \\
&\quad -\alpha_1 \epsilon^2 y_I + \alpha_1 \alpha_2 \epsilon x_I - \epsilon F_{os} \frac{P}{P_s} \\
\dot{y}_A &= \frac{1}{M_V}[F(y_{AR} - y_A) - N_A \\
&\quad +y_A(N_A + N_B) \\
&\quad +y_A(\alpha_1 \epsilon^2 y_I - \alpha_1 \alpha_2 \epsilon x_I)] \\
\dot{y}_I &= \frac{1}{M_V}[F(y_{IR} - y_I) - (\alpha_1 \epsilon^2 y_I - \alpha_1 \alpha_2 \epsilon x_I) \\
&\quad +y_I(N_A + N_B) + y_I(\alpha_1 \epsilon^2 y_I - \alpha_1 \alpha_2 \epsilon x_I)] \\
\dot{M}_L &= (N_A + N_B) + \alpha_1 \epsilon^2 y_I - \alpha_1 \alpha_2 \epsilon x_I - L \\
\dot{x}_A &= \frac{1}{M_L}[N_A - x_A(N_A + N_B) \\
&\quad -x_A(\alpha_1 \epsilon^2 y_I - \alpha_1 \alpha_2 \epsilon x_I)] \\
\dot{x}_I &= \frac{1}{M_L}[\alpha_1 \epsilon^2 y_I - \alpha_1 \alpha_2 \epsilon x_I - x_I(N_A + N_B) \\
&\quad -x_I(\alpha_1 \epsilon^2 y_I - \alpha_1 \alpha_2 \epsilon x_I)]
\end{aligned} \tag{2}
$$

In generic form, the above model becomes:

$$
\dot{x} = f(x, u^l) + \epsilon[g(x) + g^o u^o + g^p u^p] \tag{3}
$$

where u^l denotes the scaled inputs corresponding to the *large* flow rates, u^o is a scaled input corresponding specifically to the large feed flow rate, u^p is a scaled input corresponding to the *small* purge flow rate, $g(x)$ is an $O(\epsilon)$ term corresponding to the rate of inert removal from the recycle loop by mass transfer, and f, g^o, g^p are appropriately defined vector functions.

It is evident that the above model has terms of $O(1)$ and $O(\epsilon)$ which suggests potentially a two time scale behavior. In what follows, we document the two time scale feature within the framework of singular perturbations, and address the derivation of reduced-order non-stiff approximate models of the fast and slow dynamics.

3. MODEL REDUCTION

We begin with a description of the fast dynamics. This is readily obtained by considering the dynamic model of Eq.1 in the limit as $\epsilon \to 0$:

$$
\begin{aligned}
\dot{M}_R &= F_o + R - F \\
\dot{y}_{A,R} &= \frac{1}{M_R}[F_o(1 - y_{A,R}) + R(y_A - y_{A,R}) \\
&\quad -k_1 M_R y_{A,R}] \\
\dot{y}_{I,R} &= \frac{1}{M_R}[-F_o y_{I,R} + R(y_I - y_{I,R})] \\
\dot{M}_V &= F - R - (N_A + N_B) \\
\dot{y}_A &= \frac{1}{M_V}[F(y_{AR} - y_A) - N_A \\
&\quad +y_A(N_A + N_B)] \\
\dot{y}_I &= \frac{1}{M_V}[F(y_{IR} - y_I) + y_I(N_A + N_B)] \\
\dot{N}_L &= (N_A + N_B) - L \\
\dot{x}_A &= \frac{1}{M_L}[N_A - x_A(N_A + N_B)] \\
\dot{x}_I &= -\frac{1}{M_L}[x_I(N_A + N_B)]
\end{aligned} \tag{4}
$$

or in its generic form:

$$\dot{x} = f(x, u^l) \tag{5}$$

This is a non-stiff model that approximates the dynamics in the original (fast) time scale t. The steady-state conditions for this system have the form $0 = f(x, u^l)$ or more specifically:

$$\begin{aligned}
0 &= F_o + R - F \\
0 &= F_o(1 - y_{A,R}) + R(y_A - y_{A,R}) \\
&\quad -k_1 N_R y_{A,R} \\
0 &= -F_o y_{I,R} + R(y_I - y_{I,R}) \\
0 &= F - R - (N_A + N_B) \\
0 &= F(y_{AR} - y_A) - N_A + y_A(N_A + N_B) \\
0 &= F(y_{IR} - y_I) + y_I(N_A + N_B) \\
0 &= (N_A + N_B) - L \\
0 &= N_A - x_A(N_A + N_B) \\
0 &= x_I
\end{aligned} \tag{6}$$

Note that not all of these constraints (or equivalently the differential equations in Eq.4) are linearly independent. Specifically, it can be shown that there exist only 8 linearly independent constraints. This is consistent with the fact that these constraints correspond to steady state constraints in the limit as the purge flowrate *and* the feed impurity become zero. In this limit, the inert moles leaving the reactor and the condenser are identical, hence the redundant constraint.

The above observation implies that the steady state condition in this fast time scale does not specify isolated equilibrium points, but rather a one-dimensional equilibrium manifold, which confirms the presence of the two time scale behavior.

Note also that in this time scale, only the large flowrates F, R, L affect the dynamics and can be used for addressing control objectives such as stabilization of holdups, production rate and product quality. The purge flowrate has, of course, no effect on the dynamics in this fast time scale.

Turning now to the slow dynamics, let us define a slow time scale $\tau = t\epsilon$. Considering the limit $\epsilon \to 0$, we obtain a description of the slow dynamics of the form:

$$\begin{aligned}
\frac{dM_R}{d\tau} &= lim_{\epsilon\to 0}\frac{1}{\epsilon}(F_o + R - F) \\
\frac{dy_{AR}}{d\tau} &= lim_{\epsilon\to 0}\frac{1}{\epsilon M_R}[F_o(1 - y_{A,R}) \\
&\quad +R(y_A - y_{A,R}) - k_1 N_R y_{A,R}] \\
&\quad -\frac{1}{M_R}F_o\alpha_I \\
\frac{dy_{IR}}{d\tau} &= lim_{\epsilon\to 0}\frac{1}{\epsilon M_R}[-F_o y_{I,R} \\
&\quad +R(y_I - y_{I,R})] + \frac{1}{M_R}F_o\alpha_I \\
\frac{dM_V}{d\tau} &= lim_{\epsilon\to 0}\frac{1}{\epsilon}[F - R - (N_A + N_B)] \\
&\quad -F_{os}\frac{P}{P_s} \\
\frac{dy_A}{d\tau} &= lim_{\epsilon\to 0}\frac{1}{\epsilon M_V}[F(y_{AR} - y_A) - N_A \\
&\quad +y_A(N_A + N_B)] \\
\frac{dy_I}{d\tau} &= lim_{\epsilon\to 0}\frac{1}{\epsilon M_V}[F(y_{IR} - y_I) \\
&\quad +y_I(N_A + N_B)] \\
\frac{dM_L}{d\tau} &= lim_{\epsilon\to 0}\frac{1}{\epsilon}[N_A + N_B - L] \\
\frac{dx_A}{d\tau} &= lim_{\epsilon\to 0}\frac{1}{\epsilon M_L}[N_A - x_A(N_A + N_B)] \\
\frac{dx_I}{d\tau} &= lim_{\epsilon\to 0}\frac{-1}{\epsilon M_L}[x_I(N_A + N_B)]
\end{aligned} \tag{7}$$

subject to the quasi steady state constraints of Eq.6.

Note that the $O(\epsilon)$ terms in the original system description have become $O(1)$, and thus significant, in this slow time scale. Note also that the combination of $O(1)$ terms in the original model has given rise to finite, yet indeterminate limits in this slow time scale; we will denote the vector of these unknown terms by z.

In generic form, the model of the slow dynamics has the form:

$$\begin{aligned}
\frac{dx}{d\tau} &= z + g^o u^o + g^p u^p \\
0 &= f(x, u^l)
\end{aligned} \tag{8}$$

where

$$z = lim_{\epsilon\to 0}\frac{1}{\epsilon} f(x, u^l) \tag{9}$$

The model of the slow dynamics of the system comprises thus of a set of coupled differential and algebraic equations of non-trivial index, as the variables z are implicitly fixed by the quasi steady state constraints, rather than explicitly specified in the dynamic model. Indeed, this model of the slow dynamics has a well-defined index only if the flowrates u^l which appear in the algebraic constraints that determine the constraint state-space are specified as functions of the state variables x, via a control law $u^l(x)$. It can then be shown that the index of the above DAE system is exactly 2, which implies that the dimension of the underlying ODE system is 1. This system captures the slow dynamics induced by the small purge and small feed impurity, and can be used to address the control of the impurity level using the small purge stream in this slow time scale.

An explicit ODE representation of this DAE system can be obtained be employing a coordinate change of the form:

$$\begin{bmatrix} \zeta \\ \eta \end{bmatrix} = T(x) = \begin{bmatrix} \phi(x) \\ f(x, u^l(x)) \end{bmatrix} \tag{10}$$

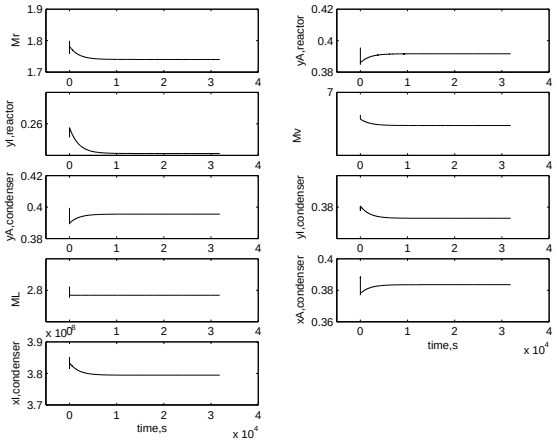

Fig. 2. Time responses of all state variables

In these new coordinates, the model of the slow dynamics has the form

$$\frac{d\zeta}{d\tau} = \frac{\partial\phi}{\partial x}z(\zeta) + \frac{\partial\phi}{\partial x}(\zeta)g^o u^o + + \frac{\partial\phi}{\partial x}(\zeta)g^p u^p \qquad (11)$$

$$\eta \equiv 0$$

Note that it is possible to chose the function $\phi(x)$ so that $\frac{\partial\phi}{\partial x}z = 0$. In this case, the variable ζ evolves independently of the 'algebraic' variables z, and is essentially a true "slow" variable in the system (whereas the original state variables exhibit both fast and slow dynamics). A meanigful choice of the function $\phi(x)$ which achieves this is $\phi(x) = M_R y_{IR} + M_V y_I$, i.e. the total impurity holdup in the recycle loop.

Notice that in the above analysis, the quantity of inert that is recycled is much larger than the inert throughput. The presence of a single slow mode associated with the inert is in complete agreement with the analysis of (Kumar and Daoutidis, 2002), which predicts a slow model of dimension equal to the number of components in the recycle loop.

4. SIMULATION STUDY

In what follows we consider a specific network of the form shown in Fig.1. The parameter values and the nominal steady states are given in Table 1. The objective is to verify the results of the analysis presented above.

As an initial simulation run, we considered an 'open-loop' experiment, whereby the three holdups are controlled by proportional controllers and we perturbed slightly the state variables from their steady state values. Fig. 2 shows the responses of all state variables. Observe that all state variables exhibit a fast transient, followed by a slow approach to steady state, which is indicative of the two time scale behavior of the system.

Table 1: Nominal values for process parameters

F_0	1.000	y_{0I}	0.0030
R	2.082	y_{AR}	0.3916
F	3.082	y_{IR}	0.2552
L	0.993	y_A	0.3955
P	$7.8{\cdot}10^{-3}$	y_I	0.3764
M_R	1.740	x_A	0.3835
M_V	6.789	x_I	$4.309 \cdot 10^{-7}$
M_L	2.784		

P-Controller gains	$K_{p,V}$	0.9	
	$K_{p,L}$	0.9	
	$K_{p,R}$	0.9	

Antoine parameters	A	B	C
for A:	15.04	273	0
for B:	15.04	273	0
for I:	17.65	273	0

ρ_L	54889	$k_A\alpha$	1
V_r	$9.25 \cdot 10^{-3}$	$k_B\alpha$	3
V_c	$5.34 \cdot 10^{-3}$	$k_I\alpha$	$1 \cdot 10^{-6}$
T_r	473	k_1	0.9
T_c	273		

Fig. 3 shows the evolution of the total inert holdup for the same simulation run; note that this variable exhibits dynamics only in the slow time scale, a fact which is consistent with it being a true slow variable.

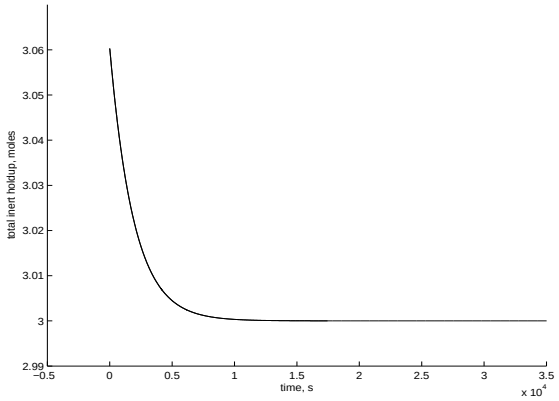

Fig. 3. Evolution of the total inert holdup

Fig. 4 illustrates the eigenspectrum of the dynamic model of the network, linearized at the nominal steady state. Observe the presence of a single eigenvalue very close to the imaginary axis, with the remaining eigenvalues further left in the complex plane.

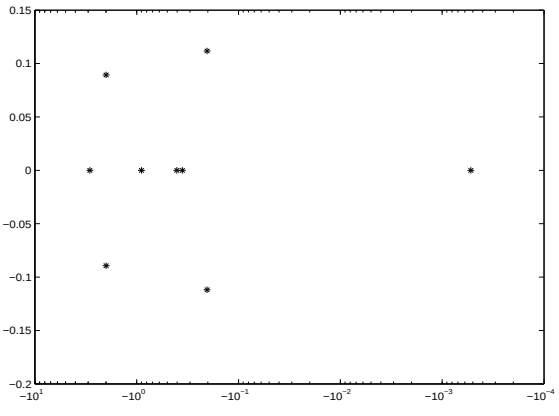

Fig. 4. Eigenspectrum of the linearized system

The model of the slow dynamics derived in the paper was used as the basis for synthesizing a nonlinear inpout/output linearizing controller which manipulates the purge flowrate to induce the following first order response for the total inert holdup ϕ :

$$\phi + \beta \frac{d\phi}{d\tau} = v \tag{12}$$

with $\beta = 4000$ and integral action imposed on the $v - \phi$ dynamics. Fig. 5 illustrates a closed-loop simulation run which illustrates the effectiveness of this controller in tracking a change in the setpoint of the inert holdup. Finally, Fig. 6 illustrates the

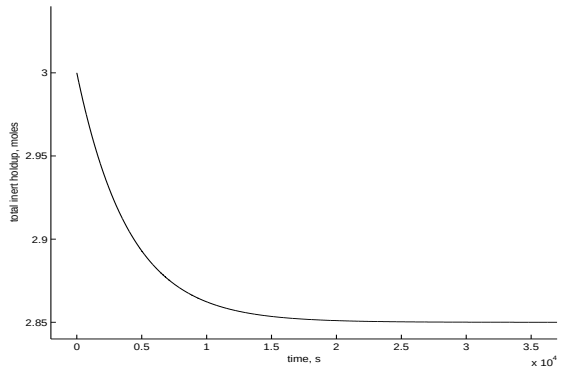

Fig. 5. Closed loop response of the controller to a 5% decrease in the inert holdup setpoint

closed-loop response of the purge flowrate for the same change in the setpoint of the inert holdup.

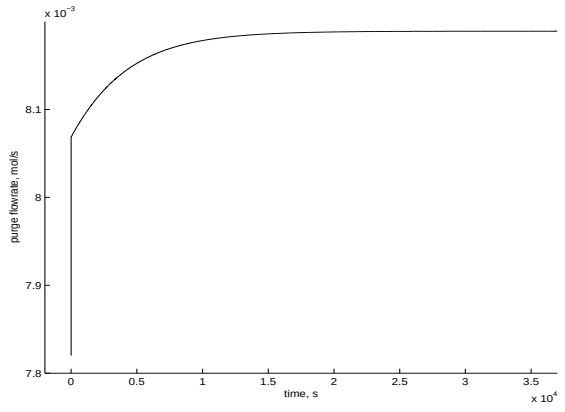

Fig. 6. Purge flowrate change for a 5% decrease in the inert holdup setpoint

5. CONCLUSIONS

In this work, we have shown that the presence of a small purge stream for the removal of an inert component from a process network with recycle, introduces a two-time scale behavior. The slow dynamics of the network was shown to be one-dimensional and directly associated with the total inert holdup. A state space realization of this slow dynamics was derived and employed in the synthesis of an input-output linearizing controller with integral action for the total inert holdup. The performance of the controller was tested by numerical simulation, indicating good setpoint tracking capabilities.

6. REFERENCES

Belanger, P. W. and W. L. Luyben (1998). Plantwide design and control of processes with inerts. 1. light inerts. *Ind. Eng. Chem. Res.* **37**(2), 516–527.

Bildea, C.S., A.C. Dimian and P.D. Iedema (2000). Nonlinear behavior of reactor-separator-recycle systems. *Comput. chem. Engng.* **24**, 209–214.

Bildea, C.S. and A.C. Dimian (1998). Stability and multiplicity approach to the design of heat-integrated pfr. *AIChE J.* **44**, 2703–2712.

Farschman, C. A., K. P. Viswanath and B. E. Ydstie (1998). Process systems and inventory control. *AIChE J.* **44**(8), 1841–1857.

Hangos, K. M., A. A. Alonso, J. D. Perkins and B. E. Ydstie (1999). Thermodynamic approach to the structural stability of process plants. *AIChE J.* **45**(4), 802–816.

Jacobsen, E. and M. Berezowski (1998). Chaotic dynamics in homogeneous tubular reactors with recycle. *Chem. Eng. Sci.* **23**, 4023–4029.

Kiss, A.A., C.S. Bildea, A.C. Dimian and P. D. Iedema (2002). State multiplicity in cstr-separator-recycle polymerization systems. *Chem. Eng. Sci.* **57**, 535–546.

Kulhavy, R., J. Lu and T. Samad (2000). Emerging technologies for enterprise optimization in the process industries. In: *Preprints of Chemical Process Control - 6.* Tucson, Arizona. pp. 411–422.

Kumar, A. and P. Daoutidis (2002). Dynamics and control of process networks with recycle. *J. Proc. Contr.* **12**, 475–484.

Luyben, M. L. and C. A. Floudas (1994). Analyzing the interaction of design and control - 2. reactor-separator-recycle system. *Comput. chem. Engng.* **18**(10), 971–994.

Luyben, W. L. (1993). Dynamics and control of recycle systems. parts 1-4.. *Ind. Eng. Chem. Res.* **32**, 466–486,1142–1162.

Luyben, W. L. (2000). Design and control of gas-phase reactor/recycle processes with riversible exothermic reactions. *Ind. Eng. Chem. Res.* **39**, 1529–1538.

Lyman, P. R. and W. L. Luyben (1996). Production rate changes in a ternary two-recycle process. *Ind. Eng. Chem. Res.* **35**(7), 2198–2203.

Marquardt, W. (2000). Fundamental modeling and model reduction for optimization based control of transient processes. In: *Preprints of Chemical Process Control - 6.* Tucson, Arizona. pp. 30–60.

Mizsey, P and I. Kalmar (1996). Effects of recycle on control of chemical processes. *Comput. chem. Engng.* **20**, S883–S888.

Morud, J. and S. Skogestad (1994). Effects of recycle on dynamics and control of chemical processing plants. *Comput. chem. Engng.* **18**, S529–S534.

Morud, J. and S. Skogestad (1998). Analysis of instability in an industrial ammonia reactor. *AIChE J.* **44**, 888–895.

Pushpavanam, S. and A. Kienle (2001). Nonlinear behavior of an ideal reactor separator network with mass recycle. *Chem. Eng. Sci.* **57**, 2837–2849.

Yi, C. K. and W. L. Luyben (1997). Design and control of coupled reactor/column systems - parts 1-3.. *Comput. chem. Engng.* **21**(1), 25–68.

YOULA–KUČERA PARAMETRISATION IN SELF–TUNING LQ CONTROL OF A CHEMICAL REACTOR

Ján Mikleš, Ľuboš Čirka, and Miroslav Fikar

Slovak University of Technology in Bratislava
Radlinského 9, 812 37 Bratislava, Slovakia
Tel: +421 2 52 49 52 69, Fax: +421 2 52 49 64 69,
e-mail: mikles@cvt.stuba.sk

Abstract: The contribution deals with the application of self–tuning LQ control of a laboratory CSTR (Continuous Stirred Tank Reactor). The strategy of the linear control system is based on a recursive identification of the dual YK (Youla–Kučera) parameter of the plant and subsequent calculation of a new YK parameter of the controller. This YK parameter is determined via a non-conventional LQ control design where squared derivative of the manipulated variable and control error are considered.

Keywords: CSTR, LQ control, Youla–Kučera parameterisation, spectral factorisation, Diophantine equation

1. INTRODUCTION

To improve the quality of the products it is necessary to improve the automation (control) of production of these products. One of the most important control problems in the chemical industry is a control of chemical reactors. Chemical reactors represent a typical class of plants with nonlinear behavior.

A traditional approach to design a control system for such plants includes nonlinear strategies (Kanter *et al.*, 2002), robust strategies (Aguilar *et al.*, 2002; Sampath *et al.*, 2002) or adaptive strategies (Dostál *et al.*, 1999).

For the most part of theoretical works reference signal is assumed to be from a class of stochastic functions. However, in technologic practice, references belong always to a class of deterministic functions. Moreover, practical needs of control show, that it is not always sufficient to restrict the output and control signals only. Very often, the manipulated variable derivatives should be restricted as well. The solution of such a control problem represents then a non-conventional LQ problem (Dostál *et al.*, 1994).

This paper describes adaptive non-conventional LQ control of the CSTR. The nonlinear model of the CSTR is for adaptive application approximated by an external SISO (Single-input Single-output) linear model and then it is possible to apply any of control techniques introduced for linear systems (Čirka *et al.*, 2002*b*; Čirka *et al.*, 2002*a*).

The main aim of this paper is to present an adaptive LQ control design involving both the controller and plant model YK parameterisations and demonstrate its feasibility on the CSTR. Dual YK parameter has been identified using IDTOOL – identification toolbox for Simulink (Čirka and Fikar, 2000). The identification algorithm has been presented in papers (Mikleš, 1990; Mikleš *et al.*, 1992).

The paper is organised as follows. Section 2 recalls the results of the Youla-Kučera parameterisation.

The simulation and experimental results obtained from control of a laboratory chemical reactor are in Section 3. Finally, Section 4 offers the conclusions.

1.1 Notation

For simplicity, the arguments of polynomials are omitted whenever possible - a polynomial $X(s)$ is denoted by X. We denote $X^*(s) = X(-s)$ for any rational function $X(s)$.

2. CONTROL ALGORITHM

Mathematical model of the reactor is described by the system of nonlinear differential equations with variable parameters. The modern control theory is the best developed for linear systems. One of the possible control solutions for nonlinear systems is to find an adequate linear mathematical approximation of the nonlinear object and to apply a self–tuning algorithm. The procedure presented here is based on the Youla–Kučera parameterisation: in each step the dual YK parameter of the plant model is estimated and subsequently a new YK parameter of the controller is designed. It is assumed that an initial plant model and stabilising controller are available.

2.1 System Description

Consider the closed-loop system illustrated in Fig. 1. A continuous-time linear time-invariant input-output nominal representation of the plant to be controlled is considered

$$Ay = Bu \tag{1}$$

where y, u are process output and controller output, respectively. A and B are polynomials in complex argument s that describe the input-output properties of the plant.

We assume that the condition $\deg B \leq \deg A$ holds (i.e. transfer function of the plant is proper) and A and B are coprime polynomials.

The reference w is considered to be from a class of functions expressed as

$$Fw = H \tag{2}$$

where H, F are coprime polynomials and $\deg H \leq \deg F$.

The feedback controller is described by the equations

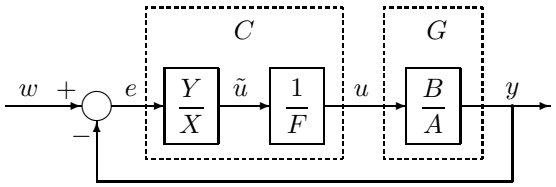

Fig. 1. Block diagram of the nominal closed-loop system

$$X\tilde{u} = Ye, \quad Fu = \tilde{u} \tag{3}$$

where X, Y are coprime polynomials and $X(0)$ is nonzero. The second equation assures that the controller tracks the class of references specified by (2).

Consider the nominal plant and the nominal controller transfer functions in the fractional representations

$$G = \frac{N_G}{D_G}, \quad C = \frac{N_C}{D_C}, \tag{4}$$

where

$$N_G = \frac{B}{M_1}, \quad D_G = \frac{A}{M_1} \tag{5}$$

$$N_C = \frac{Y}{M_2}, \quad D_C = \frac{FX}{M_2} \tag{6}$$

and M_1, $M_2 \in \mathcal{S}$ with degrees $\deg(M_1) \geq \deg(A)$ and $\deg(M_2) \geq \deg(FX)$, D_G, N_G, D_C and $N_C \in \mathcal{RH}_\infty$. $\mathcal{S}$ denotes the set of stable polynomials and $\mathcal{RH}_\infty$ the set of stable proper rational transfer functions.

A stabilising controller is then given by solution of a Diophantine equation

$$D_G D_C + N_G N_C = 1 \tag{7}$$

Substituting equations (5) and (6) into (7), the condition of stability in $\mathcal{S}$ takes the form

$$AFX + BY = M_1 M_2. \tag{8}$$

2.2 Identification Part

The identification is based on the idea which was first introduced by Hansen and Franklin (1988) in view of closed-loop experiment design. It uses the dual YK parameterisation of all linear time invariant (LTI) plants that are stabilised by a given known controller. In order to describe this method, we need the following theorem.

Theorem 1. Let a nominal model plant $G = N_G/D_G$, with N_G and D_G coprime over $\mathcal{RH}_\infty$, be stabilised by a controller $C = N_C/D_C$, with N_C and D_C coprime over $\mathcal{RH}_\infty$. Then the set of all plants stabilised by the controller C is given by

$$G(Q) = \frac{N_q}{D_q} = \frac{N_G + D_C Q}{D_G - N_C Q}, \tag{9}$$

where

$$Q \in \mathcal{RH}_\infty \tag{10}$$

Proof Dual to that of (Vidyasagar, 1985) □

Since our method involves polynomials rather than polynomial fractions, we present a short overview of the corresponding transformation between both descriptions.

Corollary 2. Let a nominal model plant $G = N_G/D_G = B/A$, with N_G, D_G, B and A defined by (5), be stabilised by a controller $C = N_C/D_C = Y/FX$, with N_C, D_C, Y and FX defined by (6). Then the set of all plants stabilised by the controller C is given by

$$G(Q) = \frac{B_q}{A_q} = \frac{B_m Q_d + F X_m Q_n}{A_m Q_d - Y_m Q_n}, \tag{11}$$

where

$$Q = \frac{Q_n}{Q_d} \in \mathcal{RH}_\infty,\ A_m = AM_2,$$
$$B_m = BM_2,\ X_m = XM_1,\ Y_m = YM_1 \tag{12}$$

Corollary 2 represents the standard parameterisation of the class of all plants that are stabilised by the actual controller C. Based on the closed-loop system in Fig. 2, Hansen and Franklin (1988) showed that the parameter Q satisfies the relation

$$z = Qx \tag{13}$$

where the signals x and z can be reconstructed by filtering the measured data u, y with filters that depend on known factors of the nominal plant P and the nominal controller C, respectively

$$x = N_G y - D_G u \tag{14}$$
$$z = D_C y + N_C u \tag{15}$$

Then, the YK parameter Q can be identified from reconstructed auxiliary signals x and z according the following prediction error equation

$$\varepsilon(t, \theta) = z(t) - Q(\theta) x(t) \tag{16}$$

where θ represents the identified parameters.

2.3 Controller Design Part

The goal of optimal deterministic LQ tracking is to design a controller that enables the control system to satisfy the basic requirements

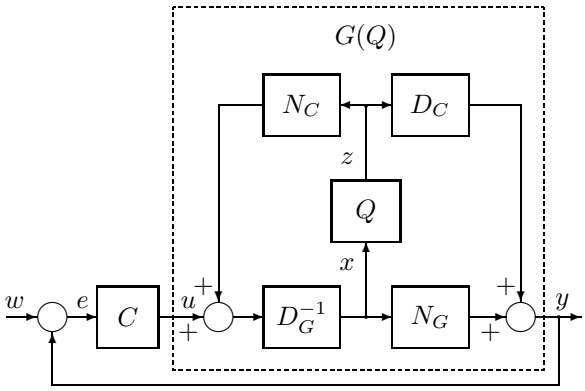

Fig. 2. The dual YK parameterisation

- stability of the closed-loop system
- asymptotic tracking of the reference

and in addition the control law that minimises the cost function

$$J = \int_0^\infty \left(\varphi \tilde{u}^2(t) + \psi e^2(t)\right) dt \tag{17}$$

where $e = w - y$ denotes the control error and $\varphi > 0$, $\psi \geq 0$ are weighting coefficients. The cost function (17) can be rewritten using Parseval's theorem, to obtain an expression in the complex domain

$$J = \frac{1}{2\pi j} \int_{-j\infty}^{j\infty} \left(\tilde{u}^* \varphi \tilde{u} + e^* \psi e\right) ds \tag{18}$$

For controller design we propose to use the method described in Čirka *et al.* (2002*b*). Let us at first summarise the known results dealing with parameterised systems:

Theorem 3. Consider the closed-loop system with the configuration in Fig. 3 defined by $G(Q)$ and $C(S)$ where $Q = Q_n/Q_d$ and $S = FS_n/S_d$ are stable proper rational functions. The closed-loop system is stable if and only if Q and S together define a stable loop.

Proof (Tay *et al.*, 1989). □

Theorem 4. Consider the minimisation of the cost function (17) with respect to the YK parameter S that is specified as a transfer function. Assume that the nominal system $G = N_G/D_G = B/A$ is stabilised by a nominal controller $C = N_C/D_C = Y/FX$ and that a stable transfer function Q is known. Solve spectral factorisation equations for stable D_c and D_f

$$D_c^* D_c = \varphi A_q^* A_q F^* F + \psi B_q^* B_q \tag{19}$$

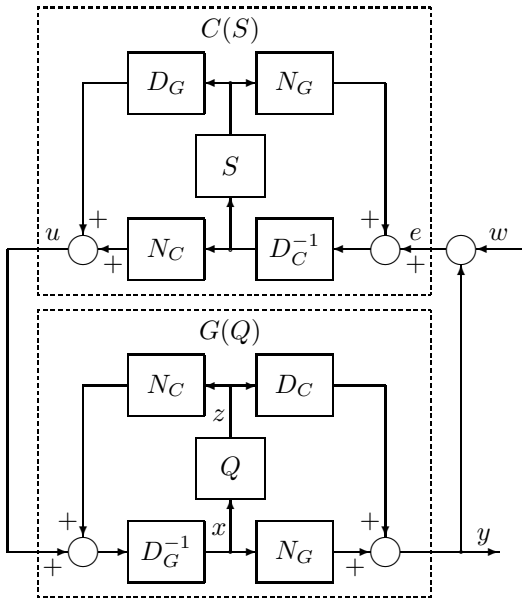

Fig. 3. Block diagram of the closed-loop system

$$D_f^* D_f = A_q^* A_q H^* H \tag{20}$$

and the coupled bilateral Diophantine equations for S_n and S_d

$$\begin{aligned} D_c^* S_n = &-\varphi D_f A_q^* F^* Y_m + \psi D_f B_q^* X_m \\ &-Q_d D V^* \end{aligned} \tag{21}$$

$$\begin{aligned} D_c^* S_d = &\varphi D_f A_q^* F^* A_m F + \psi D_f B_q^* B_m \\ &+Q_n F D V^*. \end{aligned} \tag{22}$$

The optimal YK parameter is then given as

$$S = \frac{F s_n}{s_d} = \frac{F S_n}{S_d}, \tag{23}$$

where

$$s_n = \frac{S_n}{D_c D_f} \text{ and } s_d = \frac{S_d}{D_c D_f}$$

Proof (Čirka *et al.*, 2002*b*). □

2.4 Combined Algorithm

The adaptive control algorithm is realised in the following steps:

1. Suppose the initial model $P = B/A$ is known and stabilised by a nominal controller $C = Y/X$.
2. The filtered variables x and z are obtained from equations (14) and (15).
3. The dual YK parameter Q is recursively estimated from equation (13) in the discrete time intervals $t_k = kT_s$ with the sampling period T_s. Here, the modified LDDIF (Čirka and Fikar, 2000) identification procedure was used.
4. The polynomials D_f and D_c in spectral factorisations (19) and (20) are calculated.
5. The YK parameter S is updated on the base of solution of the Diophantine equations (21) and (22).
6. Jump to step 2.

3. RESULTS AND DISCUSSION

3.1 Mathematical Model

The control algorithm has been tested on control of exothermic reactor. The mathematical model of CSTR was developed in the form (Mikleš *et al.*, 1999)

$$\begin{aligned} \frac{dc_A}{dt} &= \frac{1}{V_r}\big(q_A c_{Ai} - (q_A + q_B)c_A\big) - \upsilon \\ \frac{d\vartheta_r}{dt} &= \frac{q_A + q_B}{V_r}(\vartheta_{ri} - \vartheta_r) - \frac{A\alpha}{c_{pr} V_r \rho_r}(\vartheta_r - \vartheta_c) \\ &\quad + \frac{1}{c_{pr}\rho_r}(-\Delta H)\upsilon - \frac{k_s A\alpha}{c_{pr} V_r \rho_r}(\vartheta_r - \vartheta_{out}) \\ \frac{d\vartheta_c}{dt} &= \frac{q_c}{V_c}(\vartheta_{ci} - \vartheta_c) + \frac{A\alpha}{c_{pc} V_c \rho_c}(\vartheta_r - \vartheta_c) \end{aligned}$$

with initial conditions:
$c_A(0) = c_A^s$, $\vartheta_r(0) = \vartheta_r^s$ and $\vartheta_c(0) = \vartheta_c^s$.

The reaction rate is expressed as

$$\upsilon = 2k c_A^y c_B^z e^{\frac{E(\vartheta_r - \vartheta_0)}{R\vartheta_r\vartheta_0}}$$

$$c_B = \frac{c_{Bi} q_B}{q_A + q_B}$$

where

c	concentrations [mol m^{-3}]
V	volumes [m^3]
ϑ	temperatures [K]
ρ	densities [kg m^{-3}]
c_p	specific heat capacities [J kg^{-1} K^{-1}]
q	flow rates [m^3 min^{-1}]
A	heat exchange surface area [m^2]
α	heat transfer coeficient [J s^{-1} m^{-2} K^{-1}]
$-\Delta H$	heat of reaction [J mol^{-1}]
k	reaction rate constant [mol cm^{-3} s^{-1}]
E	activation energy [J mol^{-1}]
R	gas constant [J mol^{-1} K^{-1}]
y, z	the orders of reaction [-]
k_s	loss of heat coefficient [-]

The subscripts are $(\cdot)_r$ for the reactant mixture, $(\cdot)_c$ for the coolant, $(\cdot)_i$ for feed (inlet) values and the superscript $(\cdot)^s$ for steady-states values.

This mathematical model was tested by different identification methods and parameters in Table 1 were found. For control purposes, the controlled output and control input are defined as $y = \vartheta_r - \vartheta_r^s$ and $u = q_c - q_c^s$.

Table 1. Parameter values, inlet values and initial conditions

Values of all parameters	
V_r	$= 940\,\mathrm{cm}^3$
V_c	$= 90\,\mathrm{cm}^3$
c_{pr}	$= 4180\,\mathrm{J\,kg}^{-1}\,\mathrm{K}^{-1}$
c_{pc}	$= 4180\,\mathrm{J\,kg}^{-1}\,\mathrm{K}^{-1}$
ρ_r	$= 0.001\,\mathrm{kg\,cm}^{-3}$
ρ_c	$= 0.001\,\mathrm{kg\ cm}^{-3}$
q_A	$= 15\,\mathrm{cm}^3\,\mathrm{min}^{-1}$
q_B	$= 6\,\mathrm{cm}^3\,\mathrm{min}^{-1}$
$-\Delta H$	$= 98300\,\mathrm{J\,mol}^{-1}$
E	$= 3.0917\,10^4\,\mathrm{J\,mol}^{-1}$
k_s	$= 0.007$
k	$= 0.091\,\mathrm{mol\,cm}^{-3}\,\mathrm{s}^{-1}$
z	$= 0.875$
y	$= 1.641$
$A\alpha$	$= 116.09\,\mathrm{J\,min}^{-1}\,\mathrm{K}^{-1}$
ϑ_0	$= 297.65\,\mathrm{K}$
R	$= 8.314\,\mathrm{J\,mol}^{-1}\,\mathrm{K}^{-1}$
ϑ_{out}	$= 293.15\,\mathrm{K}$
Feed values	
ϑ_{ri}	$= 293.15\,\mathrm{K}$
ϑ_{ci}	$= 298.15\,\mathrm{K}$
c_{Ai}	$= 2.64\,10^{-3}\,\mathrm{mol\,cm}^{-3}$
c_{Bi}	$= 1.5297\,10^{-4}\,\mathrm{mol\,cm}^{-3}$
Steady-state values	
ϑ_r^s	$= 303.46\,\mathrm{K}$
ϑ_c^s	$= 303.06\,\mathrm{K}$
c_A^s	$= 1.4784\,10^{-4}\,\mathrm{mol\,cm}^{-3}$

Designed LQ adaptive control was verified in simulations as well as on the real plant. For the verification of control algorithm in laboratory conditions it was assumed with the high probability that data in Table 1 were valid in experiments, too. The results are very similar.

The goal of the adaptive control has been to track specified temperature ϑ_r in the reactor with exothermic reaction. The temperature ϑ_r is controlled by the flow rate q_c of the coolant.

The experiment was realised in two steps:

1. Control simulation of the CSTR model. The advantage of the control simulation of the chemical reaction with thermal effects is to prevent run-away problems, which can occur experimentally, particularly for such a reaction.
2. Control of real laboratory CSTR.

In both cases, the nominal transfer function of the reactor is of the form

$$G = \frac{B}{A} = \frac{-3.7}{840s + 1} \tag{24}$$

and the nominal controller is determined as

$$C = \frac{Y}{FX} = \frac{-0.117}{s} \tag{25}$$

The task was

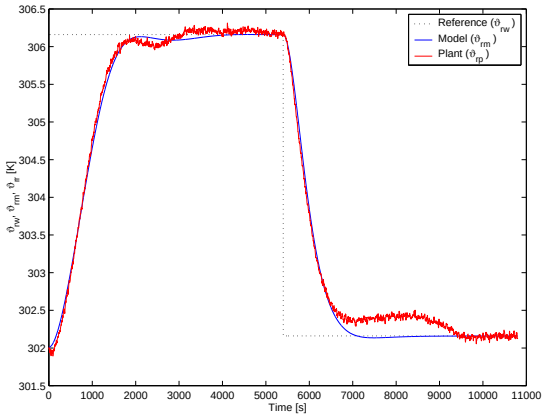

Fig. 4. Controlled output time responses

- to identify in each step the dual YK parameter of the plant (model) based on the input (the coolant feed) and output (the temperature in the reactor) data, respectively. The structure of the identified dual YK parameter was chosen of the form $Q = q_0$,
- and subsequently to design a new YK parameter of the controller.

The following references were tracked:

Step No.	1	2
Time [s]	0	5400
Temperature [K]	306.16	302.16

The boundary of the control input were used within $0 \leq u(t) \leq 140\ \mathrm{cm}^3\mathrm{min}^{-1}$. The weighting coefficients in cost (18) were $\varphi = 1$ and $\psi = 0.003$.

The obtained time responses of the temperature in the reactor (for both cases) are compared in Fig. 4. The small differences between the responses of the model and real plant were caused by the behaviour of the coolant temperature (Fig. 5) in real experiment. Fig. 6 and 7 shows simulation and experimental coolant feed and identified dual YK parameter.

Note 1. We have realised several experiments with various control structures (fixed controller and classic self-tunning controller). Both control structures performed well. However, the fixed controller cannot handle parameter changes of the reactor and its performance can deteriorate.

4. CONCLUSIONS

In this paper an adaptive LQ controller design procedure was presented. The design method is based on the idea of YK parameterisation of the controller and the plant model. The algorithm was applied to a CSTR. The advantage of this method resides in the fact that in the case of CSTR only one parameter needs to be identified in order to update the controller.

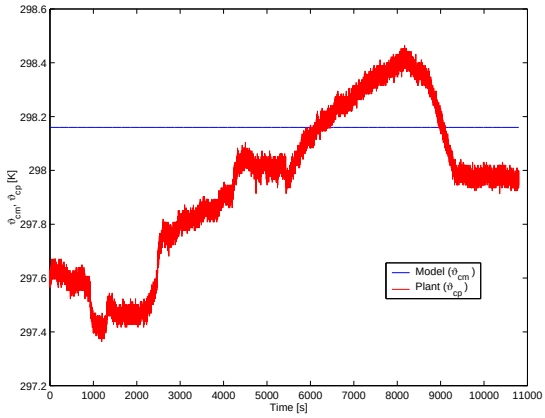

Fig. 5. Coolant temperature

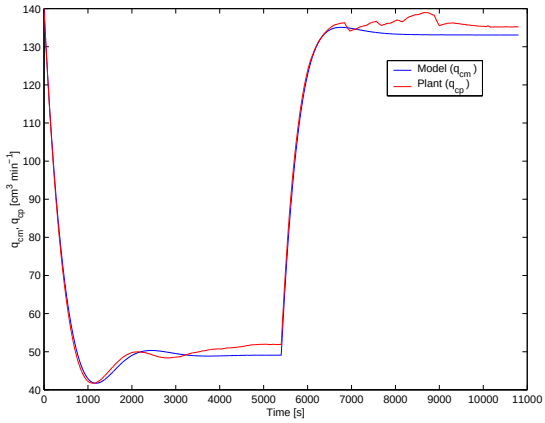

Fig. 6. Coolant feed

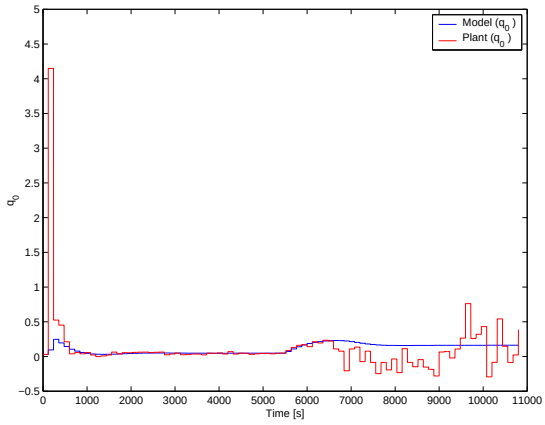

Fig. 7. Identified dual YK parameter

Acknowledgments

The authors are pleased to acknowledge the financial support of the Scientific Grant Agency of the Slovak Republic under grants No. 1/8108/01 and 1/135/03.

REFERENCES

Aguilar, R., A. Poznyak, R. Martinez-Guerra and R. Maya-Yescas (2002). Temperature control in catalitic cracking reactors via a robust PID controller. *Journal of Process Control* **12**(6), 695–705.

Čirka, Ľ. and M. Fikar (2000). IDTOOL – A dynamical system identification toolbox for MATLAB. In: *Proceedings of the 4th International Scientific – Technical Conference, Kouty nad Desnou, Czech Republic*. pp. 158–158.

Čirka, Ľ., J. Mikleš and M. Fikar (2002*a*). A deterministic LQ tracking problem: Parametrisation of the controller. *Kybernetika* **38**(4), 469–478.

Čirka, Ľ., M. Fikar and J. Mikleš (2002*b*). A deterministic LQ tracking problem: Parametrisation of the controller and the plant. *Journal of Electrical Engineering* **53**(5–6), 126–131.

Dostál, P., A. Mészáros and J. Mikleš (1994). A modified LQ tracking problem. *Journal of Electrical Engineering* **45**(4), 129–133.

Dostál, P., V. Bobál and M. Fikar (1999). One aproach to adaptive control of a continuous stirred tank reactor. *Selected Topics in Modelling and Control* **2**, 93–99.

Hansen, F. R. and G. F. Franklin (1988). On a fractional representation approach to closed-loop experiment design. In: *Proceedings American Control Conference'88, Atlanta, GA*. pp. 1319–1320.

Kanter, J. M., M. Soroush and W. D. Seider (2002). Nonlinear feedback control of multivariable non-minimum-phase processes. *Journal of Process Control* **12**(6), 667–686.

Mikleš, J. (1990). A multivariable self-tuning controller based on pole-placement design. *Automatica* **26**(2), 293–302.

Mikleš, J., H. Unbehauen and U. Keuchel (1992). Design of an adaptive continuous-time controller for multivariable systems (in German). *Automatisierungstechnik* **40**(9), 333–342.

Mikleš, J., Š. Kožka, A. Mészáros, M. Fikar and R. Keseli (1999). An iterative scheme for identification and control design with application to a chemical reactor. In: *Proceedings of the 1st EUROPOLY Workshop, Glasgow, Europoly Newsletter* **2**, *8–9*.

Sampath, V., S. Palanki, J. C. Cockburn and J. P. Corriou (2002). Robust controller design for temperature tracking problems in jacketed batch reactors. *Journal of Process Control* **12**(1), 27–38.

Tay, T. T., J. B. Moore and R. Horowitz (1989). Indirect adaptive techniques for fixed controller performance enhancement. *Int. J. Control* **50**, 1941–1959.

Vidyasagar, M. (1985). *Control System Synthesis: A Factorization Approach*. The MIT Press, Cambridge.